Long-lived circulating currents in strongly correlated nanorings

B. M. Schoenauer,[1] N. M. Gergs,[1] P. Schmitteckert,[2, 3] F. Evers,[4] and D. Schuricht[1]

[1]*Institute for Theoretical Physics, Center for Extreme Matter and Emergent Phenomena,*
Utrecht University, Princetonplein 5, 3584 CE Utrecht, The Netherlands
[2]*Institute for Theoretical Physics and Astrophysics,*
Julius-Maximilians University of Würzburg, Am Hubland, 97074 Würzburg, Germany
[3]*HQS Quantum Simulations GmbH, 76131 Karlsruhe, Germany*
[4]*Institute of Theoretical Physics, University of Regensburg, 93040 Regensburg, Germany*
(Dated: 3 July 2019)

We study the time evolving currents flowing in an interacting, ring-shaped nanostructure after a bias voltage has been switched on. The source-to-drain current exhibits the expected relaxation towards its quasi-static equilibrium value at a rate Γ_0 reflecting the lead-induced broadening of the ring states. In contrast, the current circulating within the ring decays with a different rate Γ, which is a rapidly decaying function of the interaction strength and thus can take values orders of magnitude below Γ_0. This implies the existence of a regime in which the nanostructure is far from equilibrium even though the transmitted current is already stationary. We discuss experimental setups to observe the long-lived ring transients.

Introduction.—Isolated quantum systems, such as small molecules, feature a discrete set of energy levels. When brought to contact with two electrodes, a nano-junction can form and a current begins to flow. At weak coupling, the associated level broadening, Γ_0, is still small as compared to the typical energy spacing, ΔE, of the isolated system. One might perhaps suspect that these energies by themselves set the only relevant time scales. But in fact a prominent exception is known, the Kondo phenomenon [1], which occurs in a situation where ΔE is dominated by strong on-site repulsion between the charge carriers. This suppresses charge fluctuations but allows for spin fluctuations, leading to an emergent energy scale, the Kondo temperature T_K, which is parametrically small compared to the native scales Γ_0 and ΔE.

In this work, we report another example of an emergent energy scale, Γ; it manifests in the relaxation of circulating currents in mesoscopic nanostructures. Like the Kondo temperature, the new scale is a many-body phenomenon, originating from interactions between particles on the nanostructure. However, the manifestation of the new relaxation rate Γ requires the nanostructure to be brought out of equilibrium.

A sketch of a minimal model system that exhibits the novel scale Γ is displayed in Fig. 1. Originally, similar ring-shaped devices served as a toy-models to study the interplay of interaction and interference [2, 3] and to explain quantum-interference effects in transport through functionalised graphene ribbons [4]. The ring geometry supports stationary circulating ("orbital") currents that can exceed the source-drain ("transport") current by orders of magnitude at Fermi-energies situated close to a Fano-resonance.

Strong circulating currents in ring-shaped devices, Fig. 1, generically arise as transients after a voltage quench. They then carry an oscillating amplitude with a frequency resembling the lowest lying excitation gap

of the nanostructure. We here report results from time-dependent density matrix renomalisation group (td-DMRG) [5–8] simulations showing that in situations where the interaction U is the dominating native scale of the nanoring, these oscillations can be very pronounced and very long-lived. They exhibit a lifetime Γ^{-1} that exceeds the transients in transport currents, Γ_0^{-1}, by orders of magnitude if the repulsive interaction U becomes strong. The computational finding is complemented with perturbative arguments that explain this effect and clarify the relevant physical processes. In essence, the strong suppression of Γ originates in a large energy gap between the two low-lying states and the rest of the spectrum on the nanoring (see Fig.), with ring current connecting the low-lying states. Possible experimental signatures of the effect proposed here are discussed. We note that in contrast to previously discussed [9–11] persistent ring currents driven by magnetic fields, the oscillating ring current we observe is a pure non-equilibrium effect.

Nanostructure.—The model associated with Fig. 1 is represented by the Hamiltonian $H = H_r + H_l + H_c$ de-
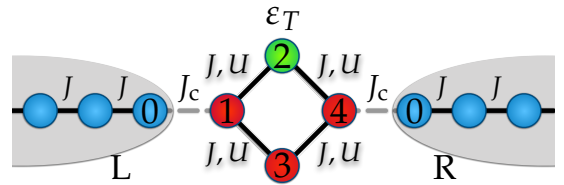

FIG. 1. Schematic representation of the nanostructure. The ring (red and green dots) is coupled by J_c to left and right leads (blue dots). Spinless fermions can hop within the ring and leads with amplitude J, the top site (site 2) on the ring is subject to the potential ε_T, and inside the ring a nearest-neighbour interaction U is present.
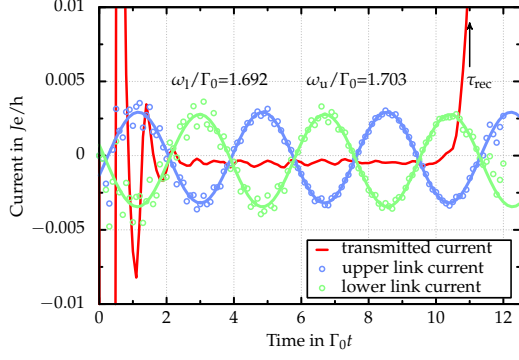
FIG. 2. Time evolution of the transmitted and ring currents, $\langle I_{\mathrm{t}}\rangle(t)$ and $\langle I_{\mathrm{r}}\rangle(t)$, evaluated using tdDMRG on the links $1 \to 2$ and $1 \to 3$ in Fig. 1. The recurrence time $\tau_{\mathrm{rec}} = L/(2v_{\mathrm{F}}) \simeq 44$ is indicated by the black arrow. While the transmitted current quickly relaxes to a stationary value, the ring currents show persistent oscillations with frequencies $\omega_{\mathrm{l,u}}$ over the accessible times. The simulation parameters are $L = 96$, $U = 4J$, $\varepsilon_T = J/2$, $J_{\mathrm{c}} = J/2$ and $eV = 0.4J$.

FIG. 3. Spectrum of the uncoupled ring H_{r} relative to the ground-state energy E_0. The ground state $|2,g\rangle$ is a CDW state with $N = 2$ particles, for $U > J$ the first excited state $|2,e\rangle$ is also a CDW state with two particles. The corresponding particle densities are shown for $U = 2J$. The observed oscillation frequencies of the ring currents match the energy difference $\varepsilon(U)$ between these two states. The higher excited states are obtained by adding or removing particles, with $\Delta(U)$ denoting the corresponding energies.

scribing the ring, the leads and their mutual coupling, respectively. The ring Hamiltonian is given by

$$H_{\mathrm{r}} = - J \sum_{\langle i,j\rangle} \left(d_i^\dagger d_j + d_j^\dagger d_i \right)$$
$$+ U \sum_{\langle i,j\rangle} \left(n_i n_j - \frac{n_i + n_j}{2} \right) + \varepsilon_T n_2, \qquad (1)$$

with operators $d_j^\dagger$ and d_j creating/annihilating spinless fermions at site j and $n_j = d_j^\dagger d_j$ denoting the corresponding density. The first term describes hopping of the fermions between nearest neighbours, while the second represents the repulsive nearest-neighbour interaction. The last term is an external potential at the top site which breaks the symmetry between the upper and lower path through the ring. The lead Hamiltonian reads

$$H_{\mathrm{l}} = -J \sum_{\alpha=\mathrm{L,R}} \sum_{n \geq 0} \left(c_{\alpha,n+1}^\dagger c_{\alpha,n} + c_{\alpha,n}^\dagger c_{\alpha,n+1} \right), \qquad (2)$$

where $c_{n,\alpha}^\dagger$ and $c_{n,\alpha}$ create and annihilate a spinless fermion at site n in the lead $\alpha=\mathrm{L,R}$. For simplicity we assume the hopping parameter J in the ring and lead to be equal. Finally, the coupling between both subsystems is facilitated by

$$H_{\mathrm{c}} = -J_{\mathrm{c}} \left(d_1^\dagger c_{\mathrm{L},0} + c_{\mathrm{L},0}^\dagger d_1 + d_4^\dagger c_{\mathrm{R},0} + c_{\mathrm{R},0}^\dagger d_4 \right), \qquad (3)$$

coupling the outer sites on the ring to the leads.

In the following we analyse the non-equilibrium currents in the nanostructure by three different methods: (i) tdDMRG simulations, (ii) a reduced density-operator transport theory (RDTT) [12, 13], and (iii) mapping to an effective two-state nanostructure [14].
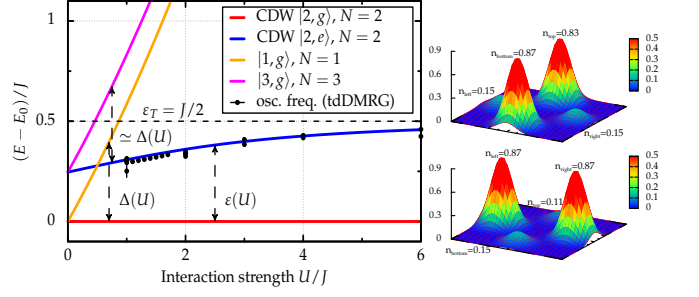
tdDMRG simulations.—First, we study the time evolution after a voltage quench using the tdDMRG algorithm [15–21]. Specially we use the time evolution scheme outlined in Refs. [8, 21, 22] performing the evaluation of the time evolution via matrix exponentials within the framework of Krylov spaces. At times $t < 0$ the system is prepared in the ground state of the model with an additional charge excess induced by a stationary gating with $V/2 \left(\sum_i n_{\mathrm{L},i} - \sum_i n_{\mathrm{R},i} \right)$. At $t = 0$ the gate is switched off, so the electrodes begin to discharge and currents start to flow through the system. We simulate the time evolution with finite leads which are long enough to be able to study the transient regime all the way into the quasi-stationary, non-equilibrium limit. Finite-size effects will interfere only at times exceeding the recurrence time $\tau_{\mathrm{rec}}=L/(2v_{\mathrm{F}})$, at which the electrons reach the boundary of the leads. (For details of the quenching protocol see Ref. [21].) Here L denotes the total number of sites, ie, the length of the leads is given by $(L - 4)/2 \approx L/2$, and $v_{\mathrm{F}} = 2J$ is the Fermi velocity of the lead electrons.

During the time evolution we determine the expectation values of the local currents $I_{\mathrm{t}} \propto \mathrm{Im}(c_i^\dagger c_{i-1})$ and $I_{\mathrm{r}} \propto \mathrm{Im}(d_k^\dagger d_l)$ flowing in the leads and the impurity, respectively, where l and k are neighbouring sites. The local current densities after quenching are displayed in Fig. 2. The transport ("transmitted") current I_{t} initially fluctuates in response to the quench for times $\Gamma_0 t \leq 3$, where we use $\Gamma_0 = 2\pi\rho_0 J_{\mathrm{c}}^2$ with the density of states in the leads $\rho_0 = 1/(2\pi J)$ as our time unit. After this transient the transmitted current appears to have reached a largely time-independent steady state in line with predictions from non-equilibrium Green function formalism [23, 24].
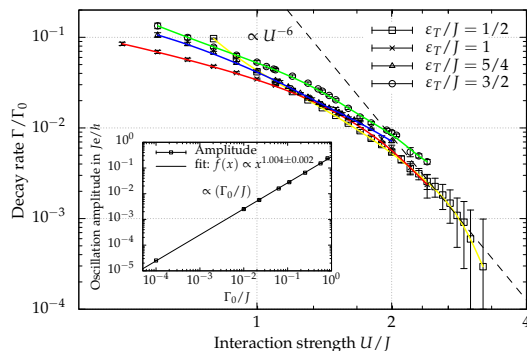
FIG. 4. Decay rate Γ of the ring current extracted from td-DMRG simulations. For $U/\varepsilon_T \simeq 1$ the decay rate appears to be exponentially suppressed in U. For $U \gg \varepsilon_T$ the decay is consistent with $\Gamma \sim U^{-6}$ predicted using an effective two-level system (5), as is indicated by the dashed line. All other parameters as in Fig. 2. Inset: Dependence of the amplitude of the ring current on the coupling Γ_0 to the leads.

In contrast, for the local currents in the ring I_r we observe a drastically different behaviour. Although some transient features decay quickly, the ring currents oscillate with a distinct frequency ω for long times. In fact, for sufficiently strong Coulomb repulsions U we do not observe a significant reduction of the oscillation amplitude within the observation times accessible to our simulations. Qualitatively similar results were obtained for a ring structure with eight sites [22].

The frequency of the oscillations can be understood based on the spectrum [22] of the uncoupled ring H_r shown in Fig. . We find that the frequency ω extracted from the tdDMRG simulations matches the energy gap between the two lowest-lying states on the ring. These two states can be identified as charge-density wave (CDW) states with $N = 2$ particles on the ring, one being the ground state $|2, g\rangle$ and the other the first excited state $|2, e\rangle$. Thus we confirm that the ring current originates from the mixing of these two states by the time evolution, which is driven by the coupling of the ring to the leads as exemplified by the proportionality of the ring current to the coupling Γ_0 shown in the inset of Fig. 5.

The decay rate Γ of the ring currents is rapidly decreasing with the interaction strength U, see Fig. 5, exhibiting a wide regime with $\Gamma \ll \Gamma_0$. To understand the origin of this regime, we proceed with the RDTT analysis.

RDTT analysis.—The RDTT [12, 13] method aims at determining the time evolution of the reduced density matrix of the nanostructure, $\rho_{ns}(t) = \mathrm{tr}_l \rho(t)$, where the trace is taken over the lead degrees of freedom in the density matrix $\rho(t)$ of the full system. The time evolution of $\rho_{ns}(t)$ can be cast in the form $\dot{\rho}_{ns}(t) = -iL_{ns}\rho_{ns}(t)$, with the effective Liouvillian L_{ns} governing the relaxation of the nanostructure. Since the ring current originates from

the mixing of the two CDW states $|2, g\rangle$ and $|2, e\rangle$, its decay is related to the decay of the off-diagonal elements ρ_{ge} and ρ_{eg} of ρ_{ns}. We have determined the corresponding decay rate from the Liouvillian L_{ns} calculated [22] to first order in the bare coupling rate Γ_0, with the perturbative regime set by $\Gamma_0 \ll T$ with the temperature T.

The obtained results for the decay rate Γ of the ring current are shown in Fig. 9(a). The results are qualitatively similar to the ones obtained via tdDMRG shown in Fig. 5 in the sense that the rate is strongly suppressed at large U. The quantitative differences between the RDTT and tdDMRG results reflect the fact that both methods operate in different parameter regimes.

Furthermore, the RDTT allows us to identify [22] the relaxation processes contributing to the decay rate, which are visualised in Fig. 9(b). The dominant processes are shown in sketches (1) and (2), which involve the tunneling of a particle off or onto the ring, while the sub-leading processes are shown in sketches (3) and (4). All processes are constraint by energetics: (1) and (2) only contribute in the regions (i) and (ii) in Fig. 9(a), (3) only in regions (i) and (iii), and (4) is relevant in the regions (i)–(iv). We stress that in region (v) no relaxation processes in order Γ_0 exist. Thus at sufficiently large interaction strengths U the rate Γ essentially drops to zero (to order Γ_0^2), explaining the very slow decay of the ring current.

Schrieffer–Wolff transformation.—Finally we focus on the regime of strong interactions, $U/\max(\varepsilon_T, J) \to \infty$, where we can derive the analytic dependence $\Gamma \sim U^{-6}$ consistent with our computational results, Fig. 5. As can be seen from the spectrum of the bare ring (Fig.), in this limit the two CDW states $|2, g\rangle$ and $|2, e\rangle$ will be well separated by an energy splitting $\Delta(U) \sim U$ from the higher excited states. It is thus instructive to construct an effective two-level system containing only these states, where the couplings to the higher excited states are treated using a Schrieffer–Wolff transformation [14] in fourth order in the couplings J and J_c. Going to this order in the expansion is necessary since all off-diagonal matrix elements exactly cancel in second order due to the mirror symmetry of the isolated ring structure [22].

The resulting two-level system can be written in the form of an electronic Kondo model, with the localised spin identified with the CDW states as $|\downarrow\rangle = |2, g\rangle$ and $|\uparrow\rangle = |2, e\rangle$ and the corresponding spin operator denoted by $\vec{S}$. An effective reservoir electronic degree of freedom can be formed via $c_{res,\uparrow\downarrow} = (c_L \pm c_R)/\sqrt{2}$ from the leads (2) of the original model; the effective spin operator formed from the first sites ($n = 0$) is denoted by $\vec{S}_{res}$. With this notation the effective model reads [22]

$$H_{SW} = \sum_{k,\sigma} \epsilon_k c_{res,k\sigma}^\dagger c_{res,k\sigma} + hS^z + \tilde{h}S^z_{res} \\ + J_\perp \left(S^x S^x_{res} + S^y S^y_{res} \right) + J_z S^z S^z_{res}, \tag{4}$$

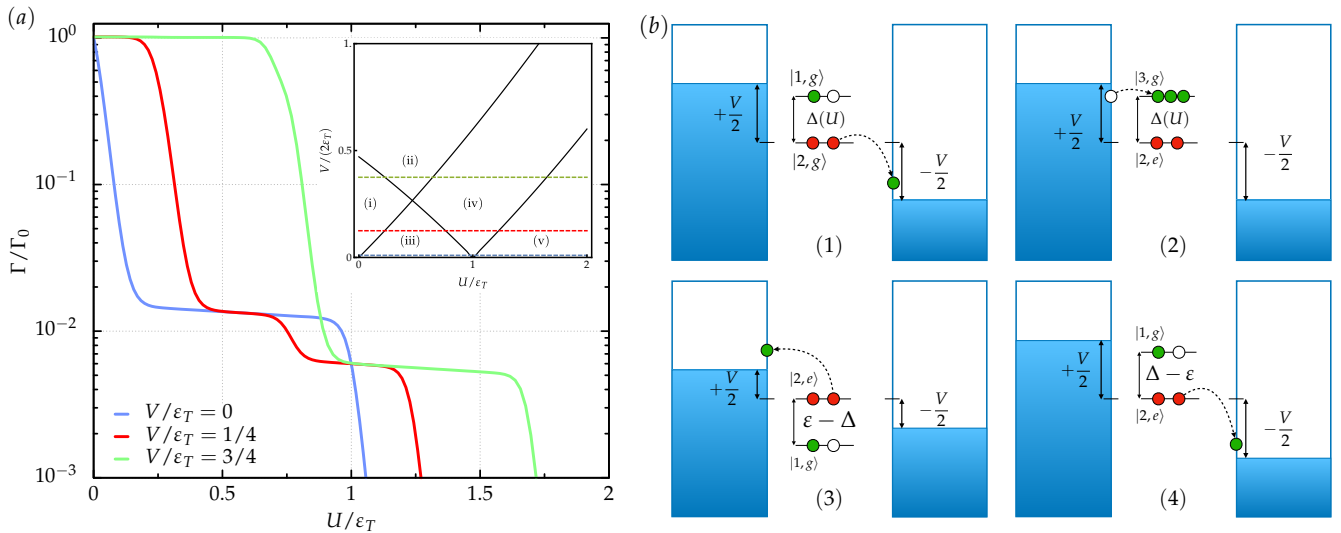where the first term is the energy of the electronic reser-

FIG. 5. (a) Decay rate Γ obtained from RDTT for the temperature $T = 10\,\Gamma_0$. Inset: In U-V-parameter space we identify five distinct regions labeled (i) to (v), in which Γ takes strongly different values. The dashed lines indicate cuts shown in the main figure. (b) Relaxation processes contributing to the rate Γ, which result in the distinct regions (i)–(v). Red and green dots represent initial and final configurations, respectively, $\Delta = \Delta(U)$ denotes the energy required to add or remove a particle (see Fig.), while $\varepsilon \approx \varepsilon_T$ is the energy gap between the two CDW states.

voir, the second and third are effective magnetic fields $h \approx \varepsilon_T$ and $\tilde{h} = \mathcal{O}(U^{-4}) \ll h$ acting on the two-level system and spin of the electron reservoir, and the fourth and fifth term represent a Kondo coupling between the two, with the coupling being strongly anisotropic with $J_z \simeq 10 J^2 J_c^2/U^3$ and $J_\perp = \mathcal{O}(U^{-5})$, and thus $|J_\perp| \ll |J_z| \ll J_c, J$.

Due to the formation of the effective reservoir electron spin from the leads L,R the bias voltage V enters the effective Kondo model in the form of a transverse field in the reservoir, ie, as $V/2 \sum_{k\sigma\sigma'} c_{\mathrm{res},k\sigma} \tau^x_{\sigma\sigma'} c_{\mathrm{res},k\sigma'}$ with τ^x being the x-component of the Pauli matrices. Finally, the ring current corresponds to oscillations between the two CDW states and thus is related to the localised spin via $I_\mathrm{r} \sim S^y$. Performing a suitable spin rotation in the electronic reservoir we calculated [22] the corresponding relaxation rate using standard perturbation theory in the Kondo system [12, 25, 26] with the result

$$\Gamma = \frac{\pi \rho_0^2 J_\perp^2}{16}\big(|\varepsilon_T + V| + |\varepsilon_T - V| + 2|\varepsilon_T|\big) + \frac{\pi \rho_0^2 J_z^2}{8} V. \quad (5)$$

We stress that in the considered regime of strong interactions this rate is vanishingly small, $\Gamma \sim \rho_0^2 J_z^2 V \sim \rho_0^2 J^4 J_c^4 V/U^6$, in accordance with our finding of long-lived oscillations in the ring current. In particular, the predicted behaviour $\Gamma \sim U^{-6}$ is consistent with our td-DMRG simulations shown in Fig. 5. We note that the result (5) is applicable deep in region (v) of Fig. 9(a), where we found that processes of order Γ_0 vanish. Furthermore, the effective model (4) will show the Kondo effect, however, the relevant energy scale T_K will be much smaller than the energy scales we consider here, in par-

ticular $T_K \ll \varepsilon_T$. Thus the equilibrium Kondo effect is not observable in our setup.

Finally we note that nanostructures with two energetically well separated low-lying states can generically be approximated by an effective Kondo model using a Schrieffer–Wolff transformation. In the absence of the above mentioned mirror symmetry the exchange couplings will be of the order $J_z, J_\perp \sim J_c^2/U \ll J_c$, resulting in a relaxation rate $\Gamma \sim \rho_0^2 J_z^2 V \sim U^{-2} \ll \Gamma_0$. Thus ring currents that couple to these low-lying states are still expected to decay very slowly.

Experimental verification.—We see a possible experimental realisation of the ring-shaped model system, Fig. 1, in molecules such as porphyrines or phthalocyanines. Single molecule conductance measurements have indeed been performed at these systems [27–29] so the possibility for bias-ramping has also been demonstrated already. As an observable indicating the slow decay of the ring currents we propose to measure the photons that are emitted when these currents decay via coupling to the radiation field. In this context we note that single-molecule electroluminscence measurements have been performed [30, 31] already and thus are indeed experimentally feasible. An alternative realisation of our ring-shaped model may be provided by quantum dot arrays [32], which in particular offer a high level of control of the couplings and allow to enter the regime of strong interactions essential for the long-lived ring currents.

Conclusion.—We have studied the relaxation of transport processes in an interacting ring-shaped nanostructure. Owing to a mirror symmetry of the Hamiltonian, the system supports oscillating ring currents long after

the transmitted current has died out, with the ratio Γ/Γ_0 of the respective relaxation rates being strongly suppressed by the interactions. Our work provides a striking example for an untypical situation in thermodynamic relaxation processes: Two observable currents approach their equilibrium values on timescales that are parametrically separated with rates differing by orders of magnitude. In addition, our system provides new insight into the field of quantum devices as we show that internal oscillations can be longer-lived than observed in currents through the system. While we have focused on a ring-shaped nanostructure, the appearance of the suppressed relaxation rate Γ is generally expected in systems that can be effectively described by a two-level model with the ring current connecting the low-lying states.

---

[1] A. C. Hewson, *The Kondo Problem to Heavy Fermions* (Cambridge University Press, Cambridge, 1993).

[2] D. Bohr and P. Schmitteckert, *The dark side of benzene: Interference vs. interaction*, Ann. Phys. **524**, 199 (2012).

[3] P. Schmitteckert, *The dark side of DFT based transport calculations*, Phys. Chem. Chem. Phys. **15**, 15845 (2013).

[4] M. Walz, J. Wilhelm, and F. Evers, *Current patterns and orbital magnetism in mesoscopic dc transport*, Phys. Rev. Lett. **113**, 136602 (2014).

[5] G. Vidal, *Efficient simulation of one-dimensional quantum many-body systems*, Phys. Rev. Lett. **93**, 040502 (2004).

[6] S. R. White and A. E. Feiguin, *Real-time evolution using the density matrix renormalization group*, Phys. Rev. Lett. **93**, 076401 (2004).

[7] A. J. Daley, C. Kollath, U. Schollwöck, and G. Vidal, *Time-dependent density-matrix renormalization-group using adaptive effective Hilbert spaces*, J. Stat. Mech. P04005 (2004).

[8] P. Schmitteckert, *Nonequilibrium electron transport using the density matrix renormalization group method*, Phys. Rev. B **70**, 121302(R) (2004).

[9] V. Meden and U. Schollwöck, *Conductance of interacting nanowires*, Phys. Rev. B **67**, 193303 (2003).

[10] R. A. Molina, D. Weinmann, R. A. Jalabert, G.-L. Ingold, and J.-L. Pichard, *Conductance through a one-dimensional correlated system: Relation to persistent currents and the role of the contacts*, Phys. Rev. B **67**, 235306 (2003).

[11] T. Rejec and A. Ramšak, *Formulas for zero-temperature conductance through a region with interaction*, Phys. Rev. B **68**, 035342 (2003).

[12] H. Schoeller, *A perturbative nonequilibrium renormalization group method for dissipative quantum mechanics*, Eur. Phys. J. Special Topics **168**, 179 (2009).

[13] R. B. Saptsov and M. R. Wegewijs, *Fermionic superoperators for zero-temperature nonlinear transport: Real-time perturbation theory and renormalization group for Anderson quantum dots*, Phys. Rev. B **86**, 235432 (2012).

[14] S. Bravyi, D. P. DiVincenzo, and D. Loss, *Schrieffer–Wolff transformation for quantum many-body systems*, Ann. Phys. **326**, 2793 (2011).

[15] D. Bohr and P. Schmitteckert, *Strong enhancement of transport by interaction on contact links*, Phys. Rev. B **75**, 241103(R) (2007).

[16] E. Boulat, H. Saleur, and P. Schmitteckert, *Twofold advance in the theoretical understanding of far-from-equilibrium properties of interacting nanostructures*, Phys. Rev. Lett. **101**, 140601 (2008).

[17] S. Kirino, T. Fujii, J. Zhao, and K. Ueda, *Time-dependent DMRG study on quantum dot under a finite bias voltage*, J. Phys. Soc. Jpn. **77**, 084704 (2008).

[18] L. G. G. V. Dias da Silva, F. Heidrich-Meisner, A. E. Feiguin, C. A. Büsser, G. B. Martins, E. V. Anda, and E. Dagotto, *Transport properties and Kondo correlations in nanostructures: Time-dependent DMRG method applied to quantum dots coupled to Wilson chains*, Phys. Rev. B **78**, 195317 (2008).

[19] F. Heidrich-Meisner, A. E. Feiguin, and E. Dagotto, *Real-time simulations of nonequilibrium transport in the single-impurity Anderson model*, Phys. Rev. B **79**, 235336 (2009).

[20] F. Schwarz, I. Weymann, J. von Delft, and A. Weichselbaum, *Nonequilibrium steady-state transport in quantum impurity models: A thermofield and quantum quench approach using matrix product states*, Phys. Rev. Lett. **121**, 137702 (2018).

[21] A. Branschädel, G. Schneider, and P. Schmitteckert, *Conductance of inhomogeneous systems: Real-time dynamics*, Ann. Phys. **522**, 657 (2010).

[22] Supplementary material.

[23] A.-P. Jauho, N. S. Wingreen, and Y. Meir, *Time-dependent transport in mesoscopic systems: general formalism and applications*, Semicond. Sci. Technol. **9**, 926 (1994).

[24] R. Tuovinen, R. van Leeuwen, E. Perfetto, and G. Stefanucci, *Time-dependent Landauer–Büttiker formula for transient dynamics*, J. Phys. Conf. Ser. **427**, 012014 (2013).

[25] A. Rosch, J. Paaske, J. Kroha, and P. Wölfle, *Nonequilibrium transport through a Kondo dot in a magnetic field: Perturbation theory and poor man's scaling*, Phys. Rev. Lett. **90**, 076804 (2003).

[26] H. Schoeller and F. Reininghaus, *Real-time renormalization group in frequency space: A 2-loop analysis of the nonequilibrium Kondo model at finite magnetic field*, Phys. Rev. B **80**, 045117 (2009); *ibid.* **80**, 209901(E) (2009).

[27] G. Sedghi, V. M. García-Suárez, L. J. Esdaile, H. L. Anderson, C. J. Lambert, S. Martín, D. Bethell, S. J. Higgins, M. Elliott, N. Bennett, J. E. Macdonald, and

R. J. Nichols, *Long-range electron tunnelling in oligo-porphyrin molecular wires*, Nat. Nanotechnol. **6**, 517 (2011).

[28] S. Schmaus, A. Bagrets, Y. Nahas, T. K. Yamada, A. Bork, M. Bowen, E. Beaurepaire, F. Evers, and W. Wulfhekel, *Giant magnetoresistance through a single molecule*, Nat. Nanotechnol. **6**, 185 (2011).

[29] A. Bagrets, S. Schmaus, A. Jaafar, D. Kramczynski, T. K. Yamada, M. Alouani, W. Wulfhekel, and F. Evers, *Single molecule magnetoresistance with combined antiferromagnetic and ferromagnetic electrodes*, Nano Lett. **12**, 5131 (2012).

[30] C. W. Marquardt, S. Grunder, A. Błaszczyk, S. Dehm, F. Hennrich, H. von Löhneysen, M. Mayor, and R. Krupke, *Electroluminescence from a single nanotube–molecule–nanotube junction*, Nat. Nanotechnol. **5**, 863 (2010).

[31] G. Reecht, F. Scheurer, V. Speisser, Y. J. Dappe, F. Mathevet, and G. Schull, *Electroluminescence of a polythiophene molecular wire suspended between a metallic surface and the tip of a scanning tunneling microscope*, Phys. Rev. Lett. **112**, 047403 (2014).

[32] U. Mukhopadhyay, J. P. Dehollain, C. Reichl, W. Wegscheider, and L. M. K. Vandersypen, *A 2×2 quantum dot array with controllable inter-dot tunnel couplings*, Appl. Phys. Lett. **112**, 183505 (2018).

Supplementary material for

Long-lived circulating currents in strongly correlated nanorings

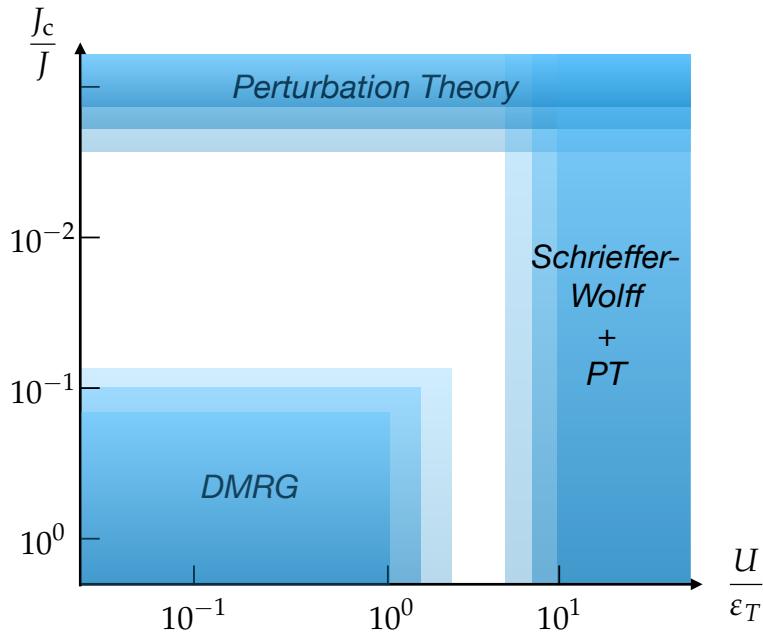B. M. Schoenauer, N. M. Gergs, P. Schmitteckert, F. Evers, D. Schuricht

FIG. 1. Parameter ranges U/ε_T and J_c/J in which our employed methods are applicable. For the DMRG time evolutions we require a coupling J_c/J between leads and impurity which is large enough to allow relaxation to the nonequilibrium steady state within the maximum simulation time $L/(2v_F)$. The coupling J_c/J also needs to be larger than the typical level splitting $2\pi J/L$. The range of interaction strengths for our DMRG method is restricted by the limitations of our fitting procedure. For large enough interaction strength the fitting error exceeds the value of the fitted decay rate. The perturbation theory (more precisely reduced density-operator transport theory) is perturbative in $\rho_0 J_c^2/T$ and therefore requires small $J_c/J \ll 1$ to be valid. The Schrieffer-Wolff transformation is perturbative in $J^2 J_c^2/U^3$. It is thus only valid in the regime $U \gg J \simeq \varepsilon_T$.

EXACT DIAGONALIZATION OF THE DECOUPLED RING IMPURITY

Spectrum and particle densities   We have performed an exact numerical diagonalization of the Hamiltonian matrix $H_r(U, \varepsilon_T, J)$ of the ring impurity in the absence of the leads. In figure 2 we plot the relative spectrum $(E - E_0)$ for the for eigenstates with the lowest energy. The energy of these states is shown as a function of the interaction strength U and a gate potential $\varepsilon_T = J/2$. The ground state features half-filling of the ring $(n = 2)$ and is indicated by the red line. The other eigenstate in the spectrum with half-filling is shown as the blue line. The state marked by the orange line features only a single electron in the ring while the state indicated by the magenta line has three electrons in the ring. For interaction $U/\varepsilon_T \geq 1$ we observe an increasing energy separation between the two eigenstates at half-filling and the rest of the spectrum. When comparing the frequency of the observed oscillations of the local currents in the ring with the relative spectrum of the ring, we find an excellent agreement of the frequencies with the energy gap between the ground state $|2, g\rangle$ and the second eigenstate at half-filling $|2, e\rangle$. The frequencies that we have obtained from the fit of a cosine function to the data of the ring current are displayed as black dots in figure 2. We show the local electron density on the ring sites for the four low energy eigenstates in figure 2. We find that the two eigenstates at half-filling exhibit characteristics of charge density waves. The ground state has a significantly increased electron density on site 1 and 4 of the ring, while the excited state features an increased density on sites 2 and 3. The other two states have a more evenly distributed electron density. We will therefore refor to the states $|2, g\rangle$ and $|2, e\rangle$ as charge density wave (CDW) states from now on.

Time evolution of an initial superposition   We have performed DMRG calculations of the time-dependent reduced density matrix of the ring impurity. We find finite occupation probabilities for both CDW states at time $t = 0$. With increasing bias voltage, the occupation probability of the excited CDW state tends to grow as well. We have used these occupation probabilities from the DMRG to construct an initial pure state

$$|\psi_0\rangle = \sqrt{N} \left(\sqrt{\rho_{gg}}|2, g\rangle \pm \sqrt{\rho_{ee}}|2, e\rangle \right) , \qquad (6)$$
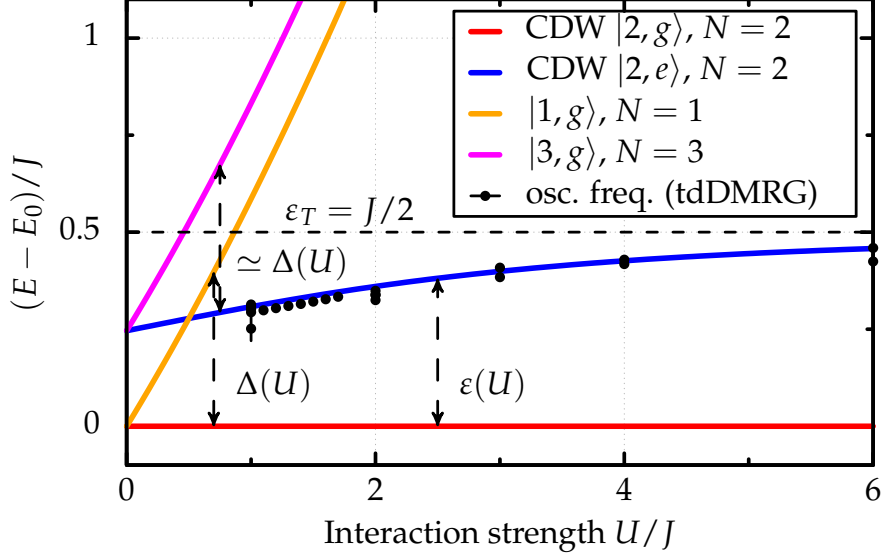
FIG. 2. Relative, low-energy spectrum of the bare ring impurity as a function of the interaction strength U/J in the repulsive regime $U > 0$. The red line indicates the ground state energy E_0. The blue line shows the energy of the excited charge density wave (CDW) state. $\varepsilon_T = J/2$ denotes the applied gate potential. The points indicate the values obtained within DMRG calculations for the oscillation frequency of the local currents inside the ring impurity.
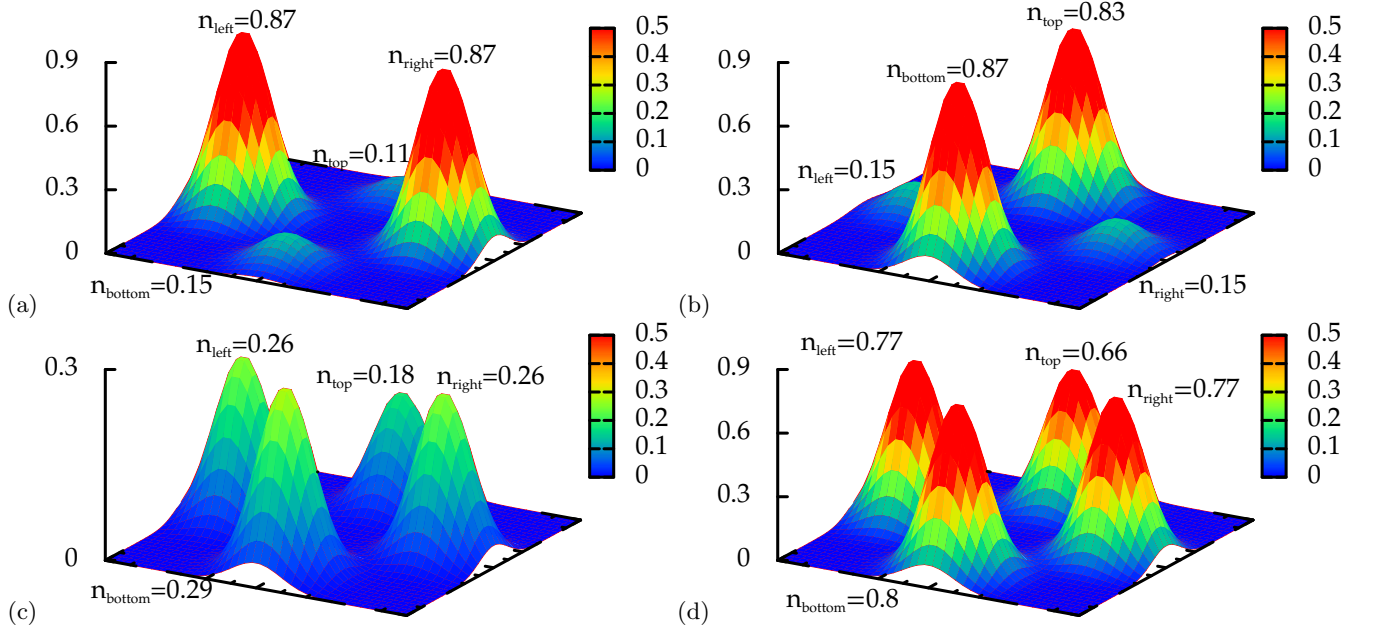
FIG. 3. Local electron density on the four lattice sites in the ring for $U/J = 2$ and $\varepsilon_T/J = 0.5$. (a) Density for $|2, g\rangle$. (b) Density for $|2, e\rangle$. We find the characteristics of charge density waves for (a) and (b). (c) Density for $|1, g\rangle$. (d) Density for $|3, g\rangle$.

where $\sqrt{N}$ is a normalization factor, ρ_{gg} refers to the ground state occupation probability and ρ_{ee} to the occupation probability of the excited CDW state. Using exact diagonalization we then perform the time evolution of this initial state in the bare ring impurity as

$$|\psi(t)\rangle = \exp(-iH_{\mathrm{r}}t)|\psi_0\rangle, \qquad (7)$$

and calculate the expectation values $\langle I_{\mathrm{u}} \rangle$ and $\langle I_{\mathrm{l}} \rangle$ of the local currents in the ring. The results of this calculation are in good agreement with our DMRG results in both amplitude and frequency.

DMRG

DMRG implementation   For our numerical calculation of the time evolution of the complete system including ring impurity and leads we have employed a typical finite lattice Density Matrix Renormalization Group (DMRG) algorithm. We keep a maximum of $N_{\mathrm{cut}} = 2800$ states per block and set the maximum amount of discarded entanglement entropy to $\delta S_{\mathrm{max}} = 10^{-7}$ in each DMRG step. We use a Krylov subspace method to calculate the matrix exponential, allowing us to chose larger time steps up to Δt of order one. Each state that is reached through application of the matrix exponential onto the initial state $|\psi_0\rangle$ is included into the density matrix from which we determine the subspace of the Hilbert that we project onto in each DMRG step. At each time step we measure the observables of interest as $\langle \psi(t)|\mathcal{O}|\psi(t)\rangle$ where the operator $\mathcal{O}$ has also been projected onto the retained subspace of the Hilbert space.

Quench protocol   At time $t = 0$ we prepare the system in the ground state of

$$H(t = 0) = H + \frac{V}{2} \left(\sum_i n_{\mathrm{L},i} - \sum_i n_{\mathrm{R},i} \right) , \tag{8}$$

and perform the time evolution using $H(t > 0) = H$. We simulate time evolution up $t \leq L/2v_F$, where L is the length of the chain (usually $L \geq 72$) and $v_F = 2J$ is the Fermi velocity of the fermions in the leads. During the time evolution we measure the expectation value of the local currents in the leads as

$$I_{\mathrm{t}} = -2eJ \left(c_i^{\dagger} c_{i-1} - \mathrm{h.c.} \right) , \tag{9}$$

and on specific bonds $1 \to 2$ and $1 \to 3$ in the ring (see Fig. 1 in the main paper) as

$$I_{\mathrm{u}} = -eJ \left(d_2^{\dagger} d_1 - \mathrm{h.c.} \right) , \tag{10}$$

$$I_{\mathrm{l}} = -eJ \left(d_3^{\dagger} d_1 - \mathrm{h.c.} \right) . \tag{11}$$

For the majority of our calculations we have used a set of default parameters, namely $L = 72$, $\varepsilon_T = J/2$, $J_{\mathrm{c}} = J/2$ and $V = 0.4 \, J/e$.

Detailed discussion of the DMRG time evolution results   In figure 4 we plot the time-dependent expectation values of the operators I_{t}, I_{u} and I_{l} using our default parameters and interaction strengths $U/J \in \{0.1, 0.5, 1.0, 2.0\}$. We begin by discussing the results for weak interaction $U/J = 0.1$ shown in figure 4 (a). For the transmitted current $\langle I_{\mathrm{t}} \rangle(t)$ we observe significant initial oscillations inside the typical transient regime $\Gamma_0 t \leq 1$ that appear to have decayed for $\Gamma_0 t > 1$ while a weak periodic oscillation remains even for large times. This periodic oscillation is not physical but a known finite size effect with a frequency $\omega \equiv V$. For the local currents in the ring we first verify that $I_{\mathrm{u}} + I_{\mathrm{l}} = I_{\mathrm{t}}$ as a consistency check of our results. For times $\Gamma_0 t \leq 1$ we find the oscillations of $\langle I_{\mathrm{u}} \rangle(t)$ and $\langle I_{\mathrm{l}} \rangle(t)$ small when compared to the oscillations of $\langle I_{\mathrm{t}} \rangle(t)$. The finite size effect with $\omega = V$ for the the local currents in the ring on the other hand is large when compared to the transmitted current. We also indicate $(\langle I_{\mathrm{u}} \rangle - \langle I_{\mathrm{l}} \rangle)/2$ as a dashed black line in fig. 4. This observable corresponds to a ring current in clockwise direction. For interaction strength $U/J = 0.5$, shown in fig. 4 (b), we solely observe quantitative differences for $\langle I_{\mathrm{t}} \rangle(t)$. While the initial transient features remain largely unchanged, the steady state current for $\Gamma_0 t > 1$ is reduced. For $(\langle I_{\mathrm{u}} \rangle - \langle I_{\mathrm{l}} \rangle)/2$ we observe what seems to be an initial oscillatory feature that is not due to finite size effect for $\Gamma_0 t < 4$. Due to the small window $1 \leq \Gamma_0 t \leq 4$ a fit does not yield reliable results for frequency and decay rate. For $U/J = 1$ the steady state value of the transmitted current experiences yet another significant reduction, whereas the transient features remain of similar size as for $U/J = 0.1$. We stil observe that the transient features of the transmitted current have largely decayed by $\Gamma_0 t = 1$. For the ring currents we find a qualitatively different behavior. The ring current exhibits periodic oscillations with a distinct frequency and a visible decay rate Γ which is an order of magnitude smaller than Γ_0. For the directional ring current $(\langle I_{\mathrm{u}} \rangle - \langle I_{\mathrm{l}} \rangle)/2$ there is even a window in which the direction of the current has changed. By increasing the interaction strength to $U/J = 2$ we find yet another decrease of the steady state trnamsitted current. In the transient regime $\Gamma_0 t \leq 1$ we now also observe an additional sign change of the transmitted current. We also no longer see the oscillations due to the finite system size. The oscillations of the local currents in the ring I_{u} and I_{l} become even more pronounced and feature a periodic change of direction. Through a fit we find that the decay rate of these oscillations
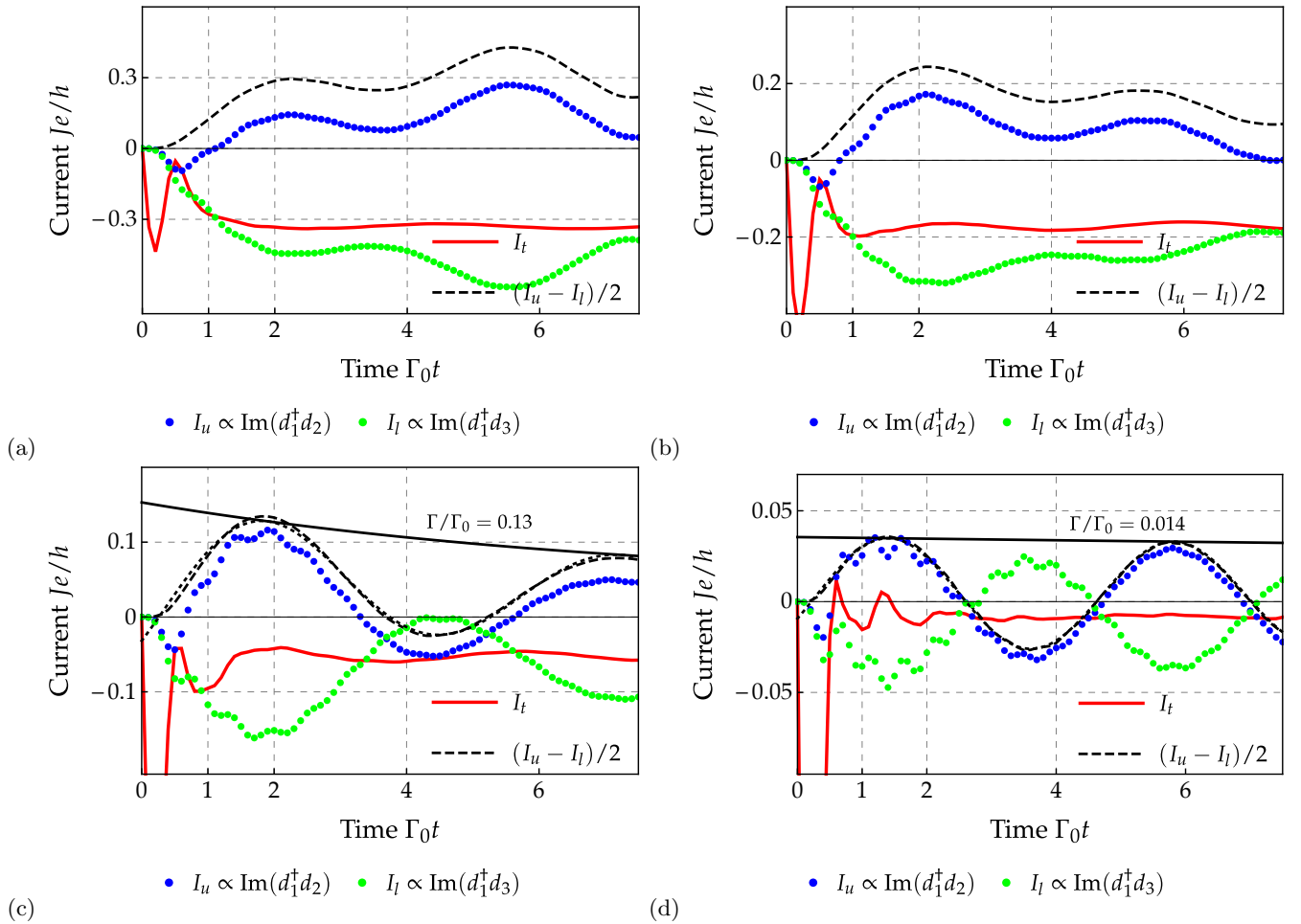
FIG. 4. Time dependent currents calculated within DMRG. The red line denotes the transport ("transmitted") current I_t. Blue dots mark the upper link current I_u and green dots the lower link current I_l. (a): $U/J = 0.1$, $\varepsilon_T/J = 0.5$, $eV/J = 0.4$, (b): $U/J = 0.5$, $\varepsilon_T/J = 0.5$, $eV/J = 0.4$, (c): $U/J = 1.0$, $\varepsilon_T/J = 0.5$, $eV/J = 0.4$, (d): $U/J = 2.0$, $\varepsilon_T/J = 0.5$, $eV/J = 0.4$. The solid black lines indicate a fit function $f(\Gamma_0 t) \propto \exp(\Gamma t)$.

is an order of magnitude smaller than in the case $U/J = 1$ and now amounts to $\Gamma/\Gamma_0 \approx 1/100$. There is a clear separation of scales between the typical decay rate Γ_0 which holds for the transmitted current and the decay rate Γ of the local currents in the ring impurity. Calculations for stronger interaction $U/J > 2$ show a continuation of this trend.

Fitting procedure for the computation of Γ To determine the oscillation frequency ε and decay rate Γ we fit a function

$$f(t) = a \exp(-\Gamma t) \cos(\varepsilon t + b) + c\,, \tag{12}$$

to our DMRG data for the local currents where Γ, ε, a, b and c are fitting parameters. The fit is performed for $\Gamma_0 < t < L/2v_F$. This fitting procedure only yields reliable results for $0.5 < U/J \leq 5$. For weak interaction $U/J \leq 0.5$ the decay time is too short to observe the amount of sine waves necessary to reliably determine the decay rate. For very strong interaction the decay rate becomes so small that it does not lead to a visible reduction in oscillation amplitude for $t < L/2v_F$. As a result, the fitting error associated with decay rate becomes larger than the decay rate itself. These limitation of the fitting procedure limit the application of our DMRG method as a tool to determine the decay rate Γ to a parameter range $0.5 < U/J \leq 5$ as indicated in figure 5.
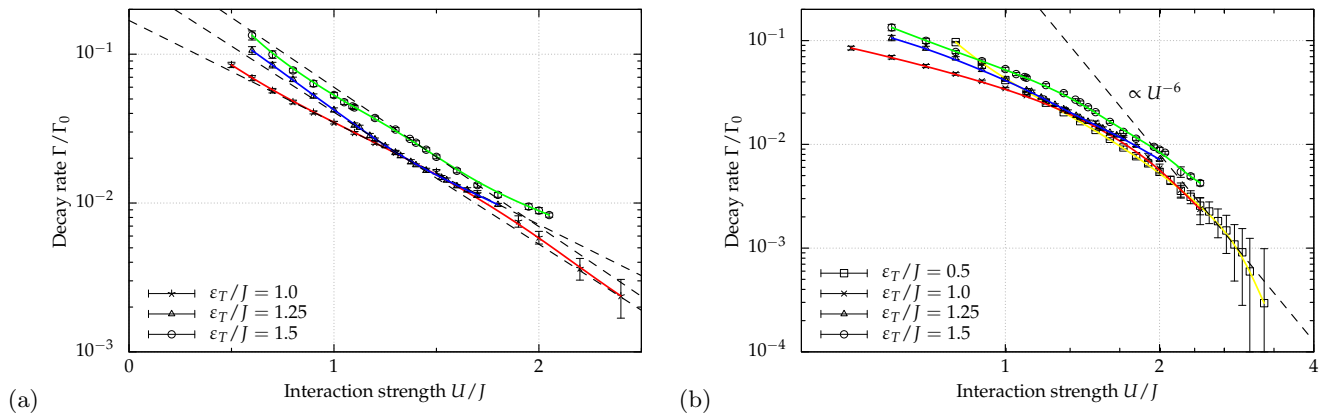
FIG. 5. Decay rate of the oscillating ring current obtained within DMRG calculations for several values of ε_T on a log-linear (a) and a log-log scale (b). We find that for $U \simeq \varepsilon$ the decay rate appears to be exponential in U whereas for $U \gg \varepsilon_T$ the decay rate exhibits an algebraic behavior. We plot a power law $f(U) \propto U^{-6}$ in (b) for comparison.

DMRG calculations for the decay rate Γ

We have performed a set of DMRG calculations to study the behavior of the decay rate Γ as a function of U/J for a range of specifically chosen parameters U, ε_T and V. The results of these calculations are shown in figures 5 (a) and (b). Due to the aforementioned limitations of our fitting procedure it is not possible to quantify Γ for $0.5 < U/J \leq 5$. In the vicinity of $U/\varepsilon_T \simeq 1$ a comparison of the log-linear and log-log plots indicates a small region of exponential suppression. For stronger interactions $U/\varepsilon_T > 1$ we observe a power law behavior of the decay rates as a function of U/J. The fit of a power law to the data indicates a smaller exponent for smaller values of ε_T. In the case of $\epsilon_T = 0.5$ we are safely in the regime $U/\epsilon_T \gg 1$ for $U/J \geq 4$. In this regime one could consider the data comparable to results obtained in the limit $U/\varepsilon_T \to \infty$. The fit of a power law finds an exponent $\alpha = 6.0 \pm 0.4$ in this case.

DMRG calculations for an eight-site ring

As a test of generality of the ring current oscillations, we have performed additional calculations for an asymmetric ring consisting of eight lattice sites. The corresponding Hamiltonian reads

$$H_{\mathrm{r},8} = -J \sum_{\langle i,j \rangle} \left(d_i^\dagger d_j + \mathrm{h.c.} \right) + U \sum_{\langle i,j \rangle} \left(n_i n_j - \frac{n_i + n_j}{2} \right) + \varepsilon_T n_4 \,, \tag{13}$$

and

$$H_{\mathrm{c}} = J_{\mathrm{c}} \left(d_1^\dagger c_{\mathrm{L},0} + d_8^\dagger c_{\mathrm{R},0} + \mathrm{h.c.} \right) \,, \tag{14}$$

where $\langle i,j \rangle$ again denotes neighboring sites, and the gate potential ε_T is now applied to the site with index $j = 4$. A sketch of the ring is shown in figure 6 (a). We plot the low-energy spectrum of the uncoupled ring, which was obtained by means of exact diagonalization, as a function of the interaction strength U/J in figure. 6 (b). Once again, we find a large separation in energy between the two lowest eigenstates ($|4,g\rangle$ and $|4,e\rangle$) and the remainder of the spectrum for $U/\varepsilon_T \gg 1$. The particular eigenstates again correspond to CDWs at half-filling, namely $N = 4$. We have performed several td-DMRG calculations in the same fashion as for the four site ring. We have chosen parameters for interaction strength U and coupling J_{c} as well as lead sizes $\ell_{\mathrm{L,R}} = (L - 8)/2$, for which we have previously observed slowly decaying ring current oscillations in the four site ring. We show the results for the time-dependent currents that have been measured in the td-DMRG calculations in figure 7. In each calculation we observe an overall increase in transient features, both for the transmitted current and the ring current $I_{\mathrm{r}} = (I_u - I_l)/2$, where $I_u = 2\mathrm{e}\,\mathrm{Im}(d_4^\dagger d_2)$ and $I_l = 2\mathrm{e}\,\mathrm{Im}(d_5^\dagger d_3)$. In case of the ring current, these transient features are modulated on top of a single dominant oscillation. These modulations increase the difficulty of fitting an exponentially decaying cosine function to the data, such that the obtained values are less reliable than in the case of the four site ring. In figure 7 (a) we find a noticable
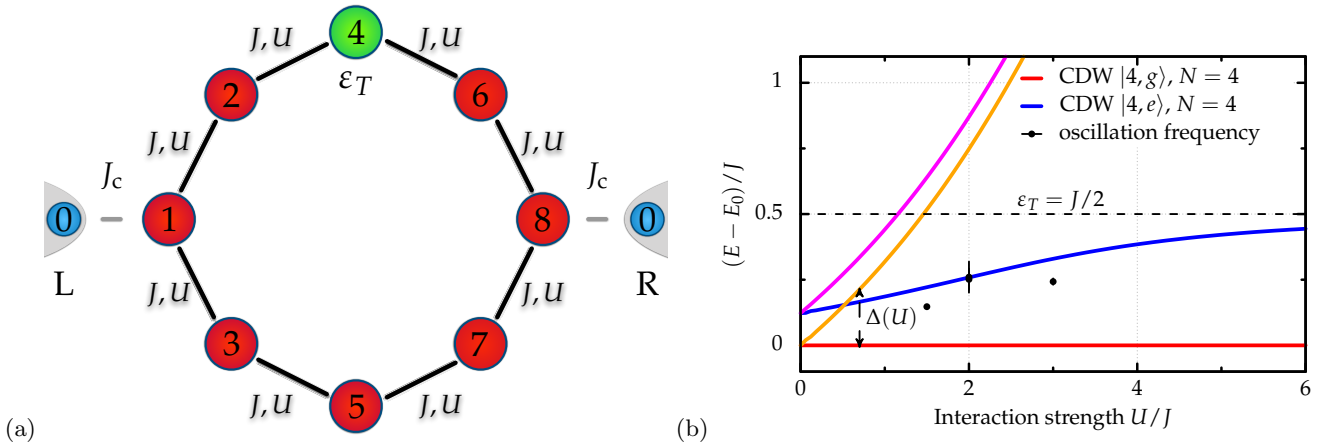
FIG. 6. (a) Schematic representation of the ring consisting of eight sites. A gate potential ε_T is applied to the site in green $j = 4$. Between neighboring sites inside the ring there is a hopping amplitude J and a repulsive fermion-fermion interaction U. The ring is connected to two tight-binding leads with an amplitude J_c. (b) Low-energy spectrum of the eight site ring disconnected from the leads as a function of the interaction strength U. The black circles indicate the fitted values for the oscillation frequency for the current data obtained with td-DMRG. As can be seen in figure 7, the fitting is accurate only for intermediate values $U = 2J$ of the interaction strength, since at weak interactions $U = 3J/2$ only one oscillation cycle has finished in the available time window, while for stronger interactions $U = 3J$ additional fast modulations appear.
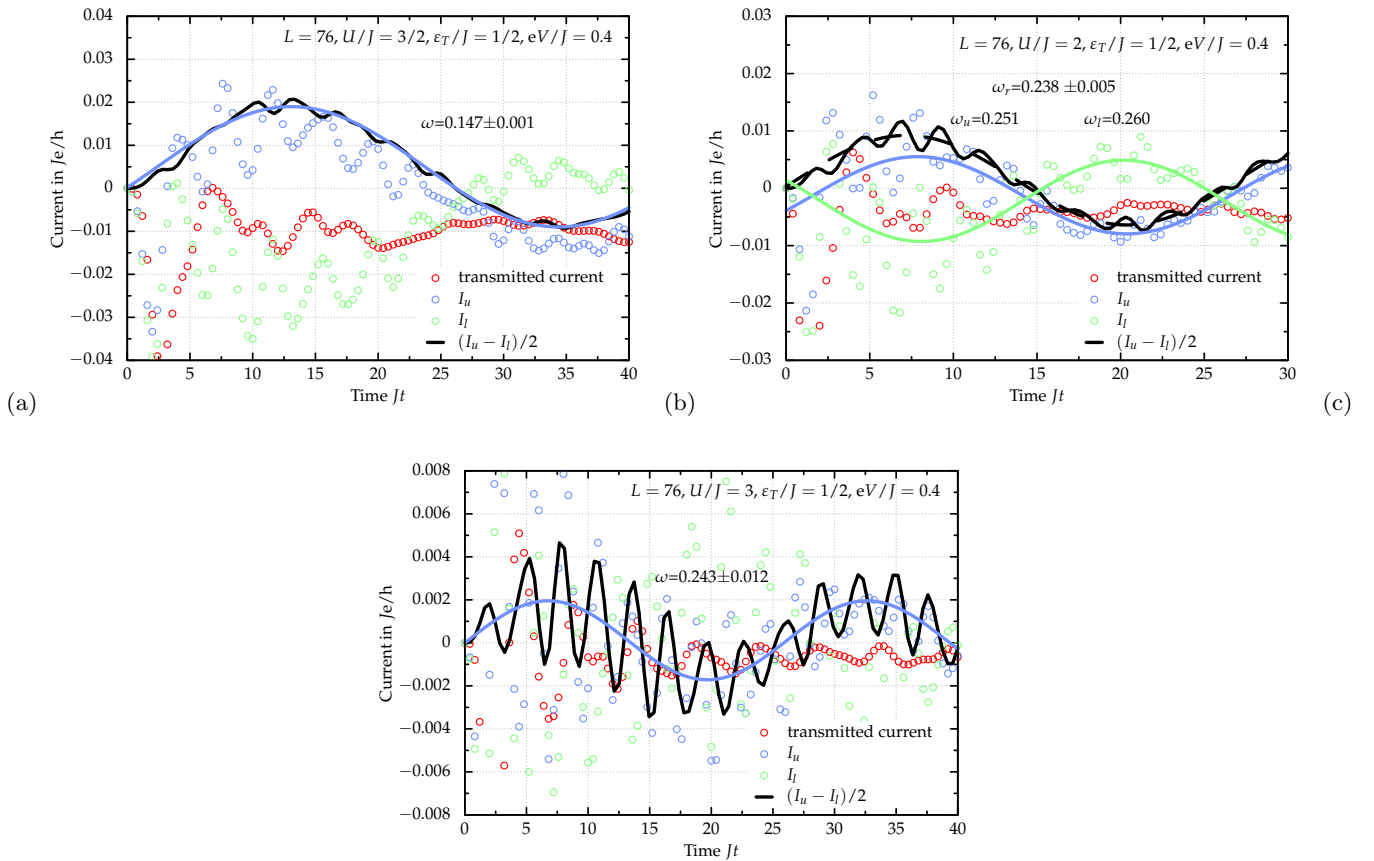
FIG. 7. td-DMRG data for the transmitted and the local currents in the ring for a system with $L = 76$ lattice sites, a ring-lead coupling $J_c/J = 0.5$, a gate potential $\varepsilon_T/J = 0.5$. A bias voltage $eV/J = 0.4$ was applied to the leads at $t = 0$. The repulsive nearest neighbor interaction is (a) $U/J = 3/2$, (b) $U/J = 2$ and (c) $U/J = 3$. For all values of the interaction strength U, we observe a slowly decaying oscillation of the ring current $I_r = (I_u - I_l)/2$ with a frequency of the order of the energy gap between ground state $|4, g\rangle$ and first excited state $|4, e\rangle$ at half-filling $N = 4$.

decay $\Gamma/J \simeq 1/100$ of the ring current oscillation within the simulation time for $U/J = 3/2$. For interaction strength $U/J = 2$ (see figure 7 (b)), the decay rate diminishes further to $\Gamma/J \simeq 1/200$. In the case $U/J = 3$, shown in figure 7 (c), other transient features of higher frequency have become significantly more pronounced. One can nevertheless still observe the underlying oscillation of frequency $\omega \simeq E_{4,e} - E_{4,g}$. A fit of an exponential decay to the data is however no longer feasible due to the other transient features. We show the fitted values for the oscillation frequencies in figure 6 (b). For $U/J = 2$ we find very good agreement. The deviation for the other values of the interaction strength, can be explained with the deficiencies of the fitting procedure.

PERTURBATION THEORY IN THE LIMIT OF SMALL HYBRIDIZATION

For our computation of the decay rate Γ, which is associated with the oscillation of the local currents in the ring, we make use of the reduced density-operator transport theory (RDTT). We mainly follow Schoeller, Eur. Phys. J. Special Topics **168**, 179 (2009). The RDTT approach is exact in the Hilbert space $\mathcal{H}_r$ of the impurity and perturbative in the hybridization between impurity and reservoirs. It may be applied if the associated perturbative scale $\Gamma_0 = 2\pi\rho_0 J_c^2$ satisfies $\Gamma_0 \ll T$, where T denotes the system temperature. The RDTT determines the time-dependent reduced density-matrix $\rho_{ns}(t)$ of an impurity by calculating corrections to the Liouvillian L of the impurity caused by tunneling processes between impurity and leads. The Liouvillian can be understood as a *superoperator* that corresponds to the action of the commutator between the Hamiltonian H and a second operator $A \in \mathcal{H}$,

$$LA \equiv [H, A]_- . \tag{15}$$

The von Neumann equation, which governs the time-evolution of the density matrix ρ, can be written in terms of the Liouvillian as

$$\dot{\rho}(t) = -i\,[H, \rho(t)]_- = -iL\rho(t)\,, \tag{16}$$

and is in turn solved by

$$\rho(t) = \exp\left[-iL(t - t_0)\right]\rho(t_0)\,. \tag{17}$$

A Laplace transform and a subsequent trace over the reservoir degrees of freedom of solution (17) yields the expression

$$\tilde{\rho}_{ns}(E) = \mathrm{tr}_l \int_{t_0}^{\infty} dt\, \exp\left[i(E - L)(t - t_0)\right]\rho(t_0)$$

$$= \mathrm{tr}_l \frac{i}{E - L_l - L_{ns} - L_V}\rho_l\rho_{ns}(t_0)\,, \tag{18}$$

where L_{ns} denotes the original Liouvillian of the impurity and L_l the Liouvillian of the reservoirs, i.e., the total Liouvillian is decomposed as $L = L_l + L_{ns} + L_V$. Expression (18) can conveniently be expanded in powers of L_V, the contribution to the Liouvillian containing the coupling between the impurity and the reservoirs. The resulting series expansion for $\tilde{\rho}_{ns}$ reads

$$\tilde{\rho}_{ns}(E) = i \sum \mathrm{tr}_l \frac{1}{E - L_l - L_{ns}} L_V \ldots L_V \frac{1}{E - L_l - L_{ns}}\rho_l\rho_{ns}(t_0)\,. \tag{19}$$

In the limit $J_c^2 \ll T$ we can set up a perturbation theory in L_V. The effective Liouvillian L_{eff} of the impurity then obtains perturbative corrections $\Sigma(E)$ that are functions of the Laplace variable E. It reads

$$L_{eff}(E) = L_{ns} + \Sigma(E)\,. \tag{20}$$

The transient features of the reduced density matrix $\rho_{ns}(t)$ are encoded in non-zero poles of

$$\frac{i}{E - L_{eff}(E)}\,. \tag{21}$$

To obtain these poles we solve for the complex roots of

$$z - L_{eff}(z)\,. \tag{22}$$

The Laplace variables $z_\pm^*$, that are roots of equation (22), have a real part that corresponds to an oscillation frequency ε of the associated transient feature and an imaginary part denoting its decay rate Γ. Our aim is to compute the particular Γ of the transient features whose frequency coincide with the frequency ε of the oscillation of the currents in the ring shaped impurity.

Properties of the Liouville space   In order to represent the Liouvillians L_{ns} and L_V as well as other superoperators G as matrices we introduce a new vector space $\mathcal{L}$ that we refer to as Liouville space. Objects that act as matrices in the Hilbert space $\mathcal{H}_{\text{r}}$ of the impurity can be thought of as vectors in this Liouville space $\mathcal{L}$. The most relevant example of such an object is the reduced density matrix ρ_{ns} of the impurity. Each matrix element $(\rho_{\text{ns}})_{i,j} = |i\rangle\langle j|$ of ρ_{ns} corresponds to a basis vector $|m)$ of the Liouville space $\mathcal{L}$. We will subsequently denote vectors in $\mathcal{H}_{\text{r}}$ as $|i\rangle$ and vectors in $\mathcal{L}$ as $|j)$. To represent each element of an operator $O \in \mathcal{H}_{\text{r}}$ as a basis vector of $\mathcal{L}$, the size of the vector space $\mathcal{L}$ has to be chosen such that $\dim(\mathcal{L}) = \dim(\mathcal{H}_{\text{r}})^2$.

Definition of the superoperators   The coupling Liovilliain L_V, which can be interpreted as the interaction vertex of the perturbation theory, induces charge fluctuations on the impurity. It has the form

$$L_V = G_1^{p_1} : J_1^{p_1} :,\tag{23}$$

where $G_1^{p_1}$ denotes the superoperator acting on the impurity and $: J_1^{p_1} :$ the normal ordered field superoperator acting on the reservoirs. The reservoir field superoperator is defined by its action on operators A acting in the reservoir Hilbert space and reads

$$J_1^p A = \begin{cases} c_1 A & p = + \\ A c_1 & p = - \end{cases},\tag{24}$$

where $1 \equiv \eta, \nu, \omega$ is a collection of indices classifying the field operator c_1 such that

$$c_1 = \begin{cases} c_{\nu,\omega}^\dagger & \eta = + \\ c_{\nu,\omega} & \eta = - \end{cases}.\tag{25}$$

Similarly we define $\bar{1} \equiv -\eta, \nu, \omega$. The action of the impurity vertex superoperator on this specific eigenvector is given by

$$G_1^p A = \begin{cases} d_1 A & p = + \\ -\sigma^p A d_1 & p = - \end{cases}.\tag{26}$$

The index p, that appears in the definition of both superoperators, determines whether the respective field operator acts on the second operator A from the left ($p = +$) or from the right ($p = -$). It can be interpreted as indicating the position of the field operator on the Keldysh contour and is thus sometimes referred to as Keldysh index. The operator σ^p accounts for fermionic sign factors. It returns a negative sign if

$$|l) = G_1^- |m) = |i\rangle\langle j|,\tag{27}$$

such that

$$\text{mod}\left[\left(\sum_i d_i^\dagger d_i |i\rangle - \sum_i d_i^\dagger d_i |j\rangle\right), 2\right] = 1.\tag{28}$$

Reservoir contractions   We perform the trace tr_{l} over the lead degrees of freedom by contracting pairs of reservoir field superoperators in our series expansion of $\tilde{\rho}_{\text{ns}}(E)$. We denote these contractions

$$\gamma_{11'}^{pp'} = \langle J_1^p J_{1'}^{p'}\rangle_{\text{eq.}},\tag{29}$$

where $\langle \ldots \rangle_{\text{eq.}}$ indicates that we assume the semi-infinite reservoirs to be in thermal equilibrium. The contractions are thus proportional to the equilibrium distribution function $f(\omega)$ at temperature T. We can simplify the subsequent calculations by separating the distribution function $f(\omega)$ into a symmetric and an antisymmetric contribution. The reservoir contraction then reads

$$\gamma_{11'}^{pp'} = \delta_{1\bar{1}'} p' \gamma_1^s + \delta_{1\bar{1}'} \gamma_1^a,\tag{30}$$

with the symmetric contribution

$$\gamma_1^s = \frac{1}{2}\rho_0,\tag{31}$$

and the antisymmetric contribution

$$\gamma_1^a = \rho_0 \left(f(\omega) - \frac{1}{2} \right),$$
(32)

where ρ_0 is the density of states in the reservoir. It is possible to absorb the Keldysh index appearing in the contraction (30) by introducing the vertices

$$\bar{G}_1 = \sum_{p=\pm} G_1^p,$$
(33)

$$\tilde{G}_1 = \sum_{p=\pm} p G_1^p.$$
(34)

Definition of the perturbative corrections   The leading order correction $\Sigma^{(1)}(E)$ to the effective impurity Liouvillian L_{eff}, which derives from charge fluctuations, has the form

$$\Sigma^{(1)}(E) = \int_{-D}^{D} d\omega_1 \sum_{p,p'=\pm} \sum_{1,1'} G_1^p \frac{1}{\omega_1 + E + \eta_1\mu_1 - L_{\text{ns}}} G_{1'}^{p'} \gamma_{11'}^{pp'}.$$
(35)

As with the reservoir contractions we can separate $\Sigma^{(1)}(E)$ in a symmetric and an antisymmetric term,

$$\Sigma^{(1)}(E) = \Sigma_s + \Sigma_a(E),$$
(36)

where Σ_s does not depend on the Laplace variable E. When using the redefined vertices $\bar{G}_1$ and $\tilde{G}_1$ we can write Σ_s as

$$\begin{aligned}
\Sigma_s &= \frac{1}{2}\rho_0 \sum_{\nu_1,\eta_1} \bar{G}_1 \int_{-D}^{D} d\omega_1 \frac{1}{\omega_1 + E + \eta_1\mu_1 - L_{\text{ns}}} \tilde{G}_{\bar{1}} \\
&= -i\frac{\pi}{2}\rho_0 \sum_{\nu_1,\eta_1} \bar{G}_1 \tilde{G}_{\bar{1}},
\end{aligned}$$
(37)

where we have integrated over all reservoir frequencies ω_1 ranging from the lower to the upper reservoir band edge D. The symmetric contribution Σ_s turns out to be entirely imaginary. It thus adds only to the decay rate of transient features but not to their oscillation frequency. The antisymmetric contribution $\Sigma_a(E)$ is a function of the Laplace variable. It reads

$$\begin{aligned}
\Sigma_a(E) &= -\frac{\rho_0}{2} \sum_{j=1}^{d(\mathcal{L})} \sum_{\nu_1,\eta_1} \int_{-D}^{D} d\omega_1 \frac{\tanh\left(\frac{\omega_1}{2T}\right)}{\omega_1 + E + \eta_1\mu_1 - \lambda_j} \bar{G}_1 |v_j)(v_j| \bar{G}_{\bar{1}} \\
&= \rho_0 \sum_{j=1}^{d(\mathcal{L})} \sum_{\nu_1,\eta_1} \left[\psi\left(\frac{1}{2} - i\frac{E + \eta_1\mu_1 - \lambda_j}{2\pi T} \right) - \log\left(\frac{D}{2\pi T} \right) \right] \bar{G}_1 |v_j)(v_j| \bar{G}_{\bar{1}},
\end{aligned}$$
(38)

where $\psi(x) = \partial_x \log(\Gamma(x))$ is the Digamma function and $|v_j)$ are the eigenvectors of the initial impurity Liouvillian L_{ns} associated with the eigenvalues λ_j of L_{ns}. The imaginary part of $\Sigma_a(E)$, which is the part contributing to the decay rate, takes a more simple, intuitive form. It reads

$$\text{Im}\left(\Sigma_a(E) \right) = -\frac{\pi}{2}\rho_0 \sum_{j=1}^{d(\mathcal{L})} \sum_{\nu_1,\eta_1} \tanh\left(\frac{E + \eta_1\mu_1 - \lambda_j}{2T} \right) \bar{G}_1 |v_j)(v_j| \bar{G}_{\bar{1}}.$$
(39)

In the basis spanned by the eigenvectors $|l\rangle$ of the impurity Hamiltonian H_{r} the initial impurity Liouvillian L_{ns} is diagonal as well and one can easily establish a one-to-one correspondence between an eigenvector $|v_j)$ of L_{ns} and a matrix element of ρ_{ns} in this eigenbasis through

$$|v_j) = |l\rangle\langle m|,$$
(40)

with the associated eigenvalue

$$\lambda_j = E_l - E_m,$$
(41)

where λ_j is the energy difference between the two eigenstates $|l\rangle$ and $|m\rangle$ of the Hamiltonian $H_{\rm r}$. There are two eigenvalues $\lambda_{\varepsilon,\pm}$ of the impurity Liovilliain $L_{\rm ns}$ that correspond to the energy difference between the two charge density wave eigenstates $|g\rangle$ and $|e\rangle$. We denote the eigenvector that corresponds to the positive eigenvalue $\lambda_{\varepsilon,+}$ as

$$|v_\varepsilon) = |2,e\rangle\langle 2,g| \,. \tag{42}$$

The action of the impurity vertex superoperators on this eigenvector is given by

$$G_1^+|v_\varepsilon) = d_1|2,e\rangle\langle 2,g| \,, \tag{43}$$

$$G_1^-|v_\varepsilon) = -(-1)|2,e\rangle\langle 2,g|d_1 \,, \tag{44}$$

where d_1 creates or annihilates a particle on lattice sites $x = 1$ or $x = 4$ of the impurity.

Perturbative diagonalization of $L_{\it eff}(E)$ While $L_{\rm ns}$ is diagonal in the eigenbasis of $H_{\rm r}$, the corrections Σ_s and $\Sigma_a(E)$ are not. Due to the large size of the Liouville space, $\dim(\mathcal{L}) = 256$, an analytical diagonalization of the effective Liouvillian $L_{\rm eff}(E) = L_{\rm ns} + \Sigma_s + \Sigma_a(E)$ is not feasible. To determine the eigenvalues of $L_{\rm eff}(E)$ we therefore treat $\Sigma_s + \Sigma_a(E)$ as perturbations to the initial Liouvillian $L_{\rm ns}$ and calculate the leading order corrections to its eigenvalues λ_j. This approximation is reasonable because $\|\Sigma_s + \Sigma_a(E)\| \leq J_{\rm c}^2 \ll \varepsilon_T \approx \lambda_j$. The eigenvalue corresponding to $|v_\varepsilon)$ is then given by

$$\lambda_\varepsilon(E) = (v_\varepsilon|L_0|v_\varepsilon) + [(v_\varepsilon|\Sigma_s|v_\varepsilon) + (v_\varepsilon|\Sigma_a(E)|v_\varepsilon)] \,. \tag{45}$$

The particle number symmetry of the impurity Hamiltonian ($[H_{\rm r},\sum_j n_j] = 0$) guarantees that $\langle 2,e|d_1|2,e\rangle \equiv 0 \equiv \langle 2,g|d_1|2,g\rangle$. We therefore find

$$(v_\varepsilon|G_1^+ G_{\bar 1}^-|v_\varepsilon) \equiv 0 \,, \tag{46}$$

$$(v_\varepsilon|G_1^- G_{\bar 1}^+|v_\varepsilon) \equiv 0 \,. \tag{47}$$

Using (46) and (47) the perturbation theory corrections from the symmetric contribution Σ_s reduce to

$$\begin{aligned}
(v_\varepsilon|\Sigma_s|v_\varepsilon) &= \sum_{\nu_1,\eta_1} -i\frac{\pi}{2}\rho_0(v_\varepsilon|[G_1^+ + G_1^-][G_{\bar 1}^+ - G_{\bar 1}^-]|v_\varepsilon) \\
&= \sum_{\nu_1,\eta_1} -i\frac{\pi}{2}\rho_0(v_\varepsilon|G_1^+ G_{\bar 1}^+|v_\varepsilon) + i\frac{\pi}{2}\rho_0(v_\varepsilon|G_1^- G_{\bar 1}^-|v_\varepsilon) \\
&= -2\pi i\rho_0 J_{\rm c}^2 = -i\Gamma_0 \,.
\end{aligned} \tag{48}$$

We see that the symmetric contribution from the leading order tunneling processes between reservoirs and impurity causes a decay rate Γ equal to the typical decay rate Γ_0 of transient features. However, this contribution does not yet factor in the fermion distribution function $f(\omega)$ in the reservoirs, meaning that each tunneling process is treated equally. The information about the distribution function is encoded in the antisymmetric correction $\Sigma_a(E)$.

Matrix elements of the antisymmetric contribution $\Sigma_a(E)$ The evaluation of the antisymmetric corrections is more involved as the contribution from each intermediate eigenstate $|v_j)$ of the Liouvillian $L_{\rm ns}$ is individually weighted by $\psi[1/2 - i(E \pm V - \lambda_j)/(2\pi T)]$. First, we identify the intermediate states $|v_j)$ that feature in the finite contributions

$$\begin{aligned}
(v_\varepsilon|\bar G_1|v_j)(v_j|\bar G_{\bar 1}|v_\varepsilon) &= (v_\varepsilon|\left[G_1^+ + G_1^-\right]|v_j)(v_j|\left[G_{\bar 1}^+ + G_{\bar 1}^-\right]|v_\varepsilon) \\
&= (v_\varepsilon|G_1^+|v_j)(v_j|G_{\bar 1}^+|v_\varepsilon) + (v_\varepsilon|G_1^-|v_j)(v_j|G_{\bar 1}^-|v_\varepsilon) \neq 0 \,.
\end{aligned} \tag{49}$$

The impurity vertex superoperator $G_{\bar 1}^\pm$ either creates or annihilates a fermion on the impurity. Finite contributions thus only involve eigenstates $|v_j)$ which satisfy $|v_j) = |m\rangle\langle 2,g|$ or $|v_j) = |2,e\rangle\langle m|$ such that $\sum_{i=1}^4 n_i|m\rangle \in \{1,3\}$. One finds in total $N = 8$ eigenstates in the Hilbert space $\mathcal{H}_{\rm r}$ with particle number $n = 1$ or $n = 3$, implying $N_L \leq 16$ finite matrix elements. A quantitative study of the matrix elements $(G_1^\pm)_{j\varepsilon}$ reveals large contributions $|(v_j|G_1^\pm|v_\varepsilon)|^2 \simeq J_{\rm c}^2$ for two eigenstates $|v_j) \in \mathcal{L}$. The two particular eigenstates are

$$|v_1^-) = |2,e\rangle\langle 1,g| \,, \tag{50}$$

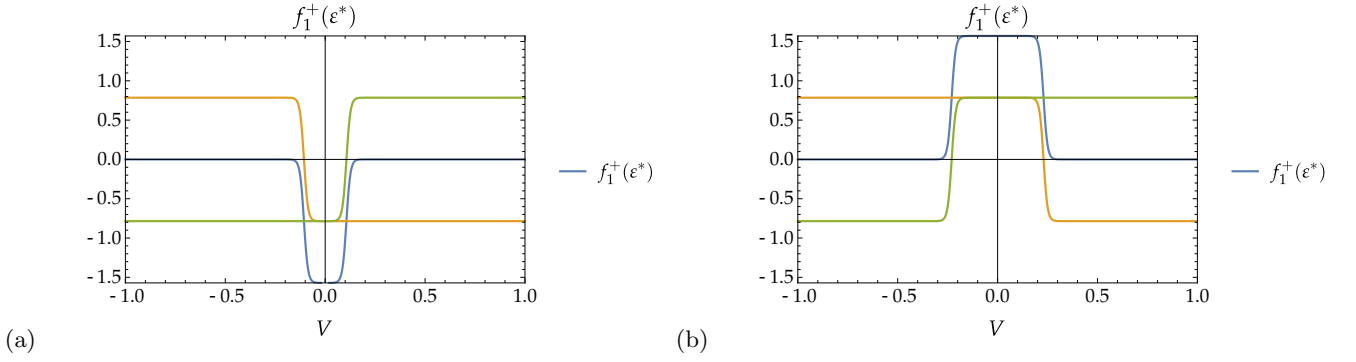$$|v_3^+) = |3,g\rangle\langle 2,g| \,, \tag{51}$$

FIG. 8. Weight function $f_1^+(\varepsilon^*, V)$ for two values of the interaction strength, (a) $U/\varepsilon_T = 0.9$ and (b) $U/\varepsilon_T = 1.2$. The orange line indicates $f(v) = -\pi \tanh[\varepsilon - \Delta + v/(2T)]/4$ and the green line $f(v) = -\pi \tanh[\varepsilon - \Delta - v/(2T)]/4$. When $U/\varepsilon_T = 1$ and $v = 0$ the weight function changes sign and leads to complete a cancellation of the symmetric and antisymmetric corrections. The weight function $f_1^+(\varepsilon^*, V)$ becomes finite if $v \leq |\varepsilon - \Delta|$. (a): $(\varepsilon - \Delta) = 0.11$, (b): $(\varepsilon - \Delta) = -0.23$.

where $|1, g\rangle$ and $|3, g\rangle$ are the two low-energy eigenstates of the impurity Hamiltonian that do not exhibit a charge density wave character and for which the energy, $E_1 = \langle 1, g|H_r|1, g\rangle < \langle 3, g|H_r|3, g\rangle = E_3$, is plotted in figure 2. The matrix elements read

$$(v_\varepsilon|G_1^-|v_1^-)(v_1^-|G_{\bar{1}}^-|v_\varepsilon) \simeq -J_c^2 \,, \tag{52}$$

$$(v_\varepsilon|G_1^+|v_3^+)(v_3^+|G_1^+|v_\varepsilon) \simeq +J_c^2 \,, \tag{53}$$

where we note that the difference in Keldysh index $p = \pm$ of the vertex superoperators G_1^p causes the opposite sign of the matrix elements. An analysis of the remaining matrix elements reveals a third matrix element that gives a sizable contribution to the self energy. Here, the intermediate state is

$$|v_1^+) = |1, g\rangle\langle g| \,, \tag{54}$$

and the matrix element evaluates to

$$(v_\varepsilon|G_1^+|v_1^+)(v_1^+|G_{\bar{1}}^+|v_\varepsilon) \simeq +\frac{J_c^2}{80} \,. \tag{55}$$

The contribution from this matrix element becomes particularly relevant in the vicinity of $U = \varepsilon_T$ due to the analytic structure of its associated weight function.

Weight function The weight function $f(\omega)$ contains the information about the fermionic distribution function $n(\omega)$ in the leads, which details the probability for an eigenstate of the lead Hmailtonian H_l with energy ω to be occupied by a fermion. Our aim is to determine the decay rate Γ which directly corresponds to the imaginary part of the the eigenvalue λ_ε of the effective Liouvillian that satisfies

$$\varepsilon^* - \lambda_\varepsilon(\varepsilon^*) = 0 \,. \tag{56}$$

The imaginary part of λ_ε originates entirely from the imaginary part of the self-energy $\Sigma(\omega)$ correction, which for the asymmetric correction $\Sigma_a(\omega)$ stems from the weight function $f_j^\pm(\omega)$. The imaginary part of the weight function evaluated at the eigenvalue ε^* has the simple form

$$f_j(\varepsilon^*) = -i\frac{\pi}{2} \sum_{\eta_1 = \pm} \tanh\left(\frac{\varepsilon^* + \eta_1\frac{V}{2} - \lambda_j}{2T}\right) \,, \tag{57}$$

We know that $\varepsilon^* \simeq E_e - E_g$. We can thus also express the weigth function as

$$f_j(\varepsilon^*) = -i\frac{\pi}{2} \sum_{\eta_1 = \pm} \tanh\left(\frac{E_e - E_g - \lambda_j + \eta_1\frac{V}{2}}{2T}\right) \,. \tag{58}$$

The eigenvalues λ_j that correspond to the three largest matrix elements read

$$\lambda_1^+ = E_1 - E_g \equiv \Delta\,, \tag{59}$$

$$\lambda_3^+ = E_3 - E_g = E_3 - E_e + E_e - E_g \simeq \varepsilon + \Delta\,, \tag{60}$$

$$\lambda_1^- = E_e - E_1 = E_e - E_g + E_g - E_1 \simeq \varepsilon - \Delta\,, \tag{61}$$

It is easy to see that, depending on the eigenvalue λ_j, either the dependence on E_g or E_e is removed from the argument of the weight function. To simplify the expression we introduce $v \equiv |V/2|$. The weight function then reads

$$f_j(\varepsilon^*) = -i\frac{\pi}{2}\rho_0 \left[\tanh\left(\frac{\varepsilon - \lambda_j + v}{2T}\right) + \tanh\left(\frac{\varepsilon - \lambda_j - v}{2T}\right)\right]\,. \tag{62}$$

In the limit $T \ll \{J, U, \varepsilon, D\}$ we can approximate the weight function as

$$f_j(\varepsilon^*) = -i\frac{\pi}{2}\rho_0 \left[\text{sign}(\varepsilon - \lambda_j + v) + \text{sign}(\varepsilon - \lambda_j - v)\right]\,. \tag{63}$$

When evaluating this approximation for the three relevant eigenvalues $\lambda_j^{\pm}$ one finds

$$f_1^+(\varepsilon^*) = -i\frac{\pi}{2}\rho_0 \left[\text{sign}(\varepsilon - \Delta + v) + \text{sign}(\varepsilon - \Delta - v)\right] \tag{64}$$

$$= -i\frac{\pi}{2}\rho_0 \left[\theta(\varepsilon_T - U)(1 + \text{sign}(\varepsilon - \Delta - v)) + \theta(U - \varepsilon_T)(\text{sign}(\varepsilon - \Delta + v) - 1)\right]\,,$$

$$f_3^+(\varepsilon^*) = -i\frac{\pi}{2}\rho_0 \left[\text{sign}(-\Delta + v) + \text{sign}(-\Delta - v)\right] \tag{65}$$

$$= -i\frac{\pi}{2}\rho_0 \left[\text{sign}(v - \Delta) - 1\right]\,,$$

$$f_1^-(\varepsilon^*) = -i\frac{\pi}{2}\rho_0 \left[\text{sign}(\Delta + v) + \text{sign}(\Delta - v)\right] \tag{66}$$

$$= -i\frac{\pi}{2}\rho_0 \left[1 + \text{sign}(\Delta - v)\right]\,,$$

where we note that $\varepsilon, \Delta \geq 0$.

Decay channels The three matrix elements $(v_\varepsilon|G_1^-|v_1^-)(v_1^-|G_{\bar{1}}^-|v_\varepsilon)$, $(v_\varepsilon|G_1^+|v_3^+)(v_3^+|G_{\bar{1}}^+|v_\varepsilon)$ and $(v_\varepsilon|G_1^+|v_1^+)(v_1^+|G_{\bar{1}}^+|v_\varepsilon)$ correspond to four different decay channels that cause the decoherence of a state of the form $|\psi\rangle = \alpha|2, g\rangle + \beta|2, e\rangle$. A schematic of these decay channels is shown in figure 10. We now turn to the discussion of the decay channels and why they become suppressed for specific sets of parameters U, ε_T and V.

$(v_\varepsilon|G_1^-|v_1^-)(v_1^-|G_{\bar{1}}^-|v_\varepsilon)$: An electron is ejected from the ring impurity, which has initially been in the ground state $|2, g\rangle$. Due to the particle hole symmetry of the repulsive nearest neighbor interaction U, this requires the energy $\Delta(U)$. Said energy needs to be supplied by the increase of chemical potential energy μ, which the electron gains by entering the metallic lead. The process is thus only possible if $\mu = -V/2 < -\Delta(U)$. Here, we have assumed that the electron can only enter the lead to which a negative chemical potential $-V/2\sum_k n_k$ was applied. The condition is reflected by the weigth function $f_1^-(\varepsilon^*)$, which evaluates to zero if v surpasses Δ. Then the imaginary part of the asymmetric correction $\Sigma_a(\omega)$ does not compensate the constant imaginary part of the symmetric correction Σ_s for this decay channel. A sketch of the decay process is shown figure 10 (1), where red in indicates the initial and green the final configuration of the decay process.

$(v_\varepsilon|G_1^+|v_3^+)(v_3^+|G_{\bar{1}}^+|v_\varepsilon)$: An electron tunnels onto the ring impurity, which has initially been in the excited charge density wave state $|2, e\rangle$. The additional electron increases the interaction energy on the ring impurity by $\Delta(U)$. This energy has to be supplied by the additional electron. The process is thus only possible if the chemical potential in the lead that the electron originates from satisfies $\mu = V/2 > \Delta(U)$. As with the previous matrix element, $f_3^+(\varepsilon^*)$ vanishes once $v > \Delta$ such that the constant negative imaginary part of the symmetric correction Σ_s is not compensated. We display a sketch of this decay channel in figure 10 (2).

The decay channels $(v_\varepsilon|G_1^-|v_1^-)(v_1^-|G_{\bar{1}}^+|v_\varepsilon)$ and $(v_\varepsilon|G_1^+|v_3^+)(v_3^+|G_{\bar{1}}^+|v_\varepsilon)$ are closely related - one involves the ground state while the other one involves the excited state - and are thus respectively allowed or suppressed in the same parameter regimes.

$(v_\varepsilon|G_1^+|v_1^+)(v_1^+|G^+|v_\varepsilon)$: An electron tunnels out of the ring impurity, which has initially been in the excited charge density wave state $|2, e\rangle$. Depending on the interaction strength U, this tunneling process is energetically favorable or unfavorable. For $U < \varepsilon_T$ the one particle state $|1, g\rangle$ is lower in energy than $|2, e\rangle$. Since the electron
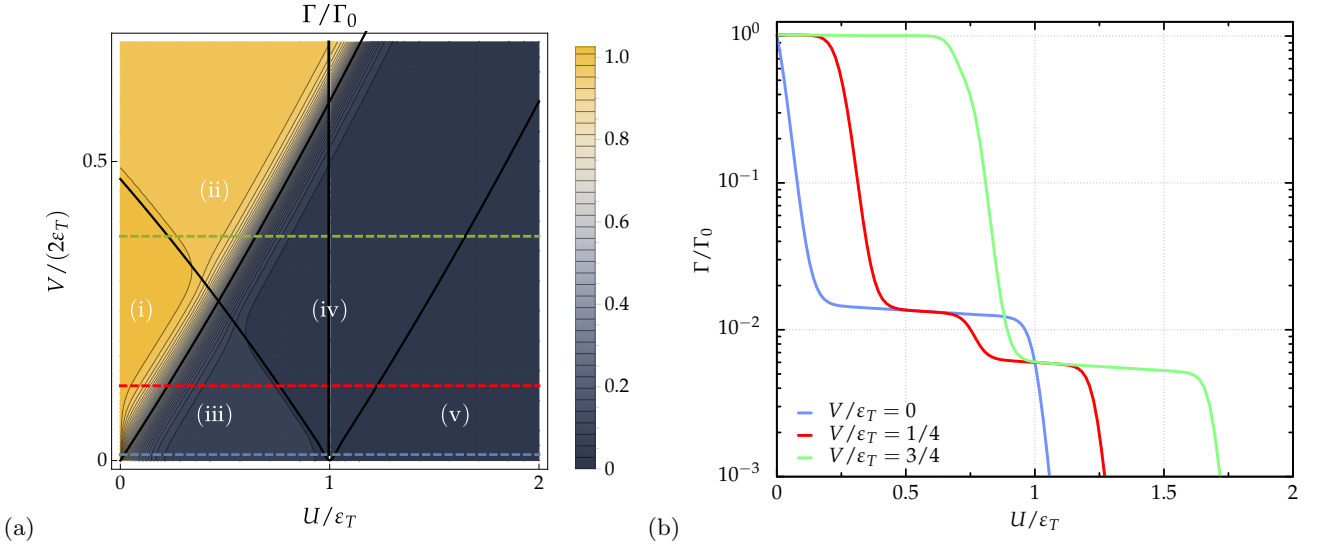
FIG. 9. (a) Perturbation theory results for the decay rate $\Gamma = \text{Im}[\lambda_\varepsilon(\varepsilon^*)]$ of the transient feature with oscillation frequency ε as a function of the interaction strength U/ε_T and bias voltage $V/(2\varepsilon_T)$ in units of Γ_0. We observe five distinct sectors $[(i) - (v)]$ in which the decay rate assumes different values. These sectors are characterized by their available decay channels. In sector (i) the decay rate Γ exceeds Γ_0 due to the presence of an unconventional decay channel, see fig. 10 (3). For $V/(2\varepsilon_T) < \Delta$ we find the dominant decay channels suppressed, leading to a decrease of the decay rate Γ by an order of magnitude compared to Γ_0. In sector (v) each decay channel is suppressed leading to an effective decay rate $\Gamma/\Gamma_0 \to 0$. (b) shows the decay rate Γ/Γ_0 as a function of U/ε_T for three distinct values of the bias voltage V. The chosen parameters are indicated by the blue, red and green dashed lines in (a).

can carry this excess energy it can tunnel into either lead as long as $\mu = V/2 < \varepsilon - \Delta$. Having two effective decay channels, one for each lead, increases the decay rate as can be seen in sector (i) and (iii) of figure 9. The weight function reflects this as $f_1^+(\varepsilon^*) = -i\pi\rho_0$, which adds to the imaginary part of the symmetric correction $\Sigma_s \propto -i\pi\rho_0$ instead of compensating for it. A schematic of this process is shown in figure 10 (3) and (4). For $U > \varepsilon_T$ the state $|1, g\rangle$ becomes higher in energy than $|2, e\rangle$. For an electron to tunnel out of the ring additional energy is now required. This energy needs to be provided by the increase in chemical potential energy μ that the electron gains by entering the lead. The tunneling process is thus only possible if $\mu = -V/2 < -(\Delta - \varepsilon)$. We sketch this process in figure 10 (4).

For $U > \varepsilon_T$ and $v < \Delta - \varepsilon$ each decay channel becomes suppressed and we find

$$\text{Im}[\Sigma_a(\varepsilon^*)] \equiv -\text{Im}[\Sigma_s] . \tag{67}$$

The first order corrections to the imaginary part of the transient feature with oscillation frequency ε^* therefore vanish entirely.

Discussion of the phase diagram In figure 9 we plot the decay rate Γ/Γ_0 of the eigenvalue $\lambda_\varepsilon(\varepsilon^*)$ as a function of the ratios U/ε_T and $V/(2\varepsilon_T)$. We identify five different sectors of these ratios in which the decay rate Γ take different values due to the presence or absence of the previously outlined decay channels respectively. In sector (i) we find the presence of the decay channels (1), (2), (3) and (4). The decay channel (3) does not exist for many of the typical quantum dot systems. Its presence leads to a decay rate Γ that exceeds the typical level broadening Γ_0. By increasing the bias voltage V one crosses from sector (i) into sector (ii) where the decay channel (3) becomes suppressed as there is no remaining unoccupied state with energy $\omega = \varepsilon_F + (\varepsilon - \Delta)$ available in the left lead . In sector (ii) we find $\Gamma = \Gamma_0$. By increasing the interaction strength U/ε_T sufficiently one passes from sector (ii) into sector (iv). The increase in interaction strength causes an increased energy gap $\Delta(U)$. As soon as $\Delta(U) > V/2$ both the decay channels (1) and (2) simultaneously become suppressed. This leads to a significant reduction of the decay rate by almost two orders of magnitude such that $\Gamma \leq \Gamma_0/80$. For $U/\varepsilon_T < 1$ the reduction of the bias voltage facilitates a crossover from sector (iv) into sector (iii). In this sector, the decay channel (3) is no longer suppressed leading to small increase of $\Delta\Gamma \simeq \Gamma_0/80$. For $U/\varepsilon_T > 1$ and $V/(2\varepsilon_T) < (\Delta - \varepsilon)$ every decay channel is suppressed as is shown in sector (v). The corresponding decay rate becomes $\Gamma/\Gamma_0 \to 0$. For a finite decay rate, higher order perturbation theory corrections would be required.
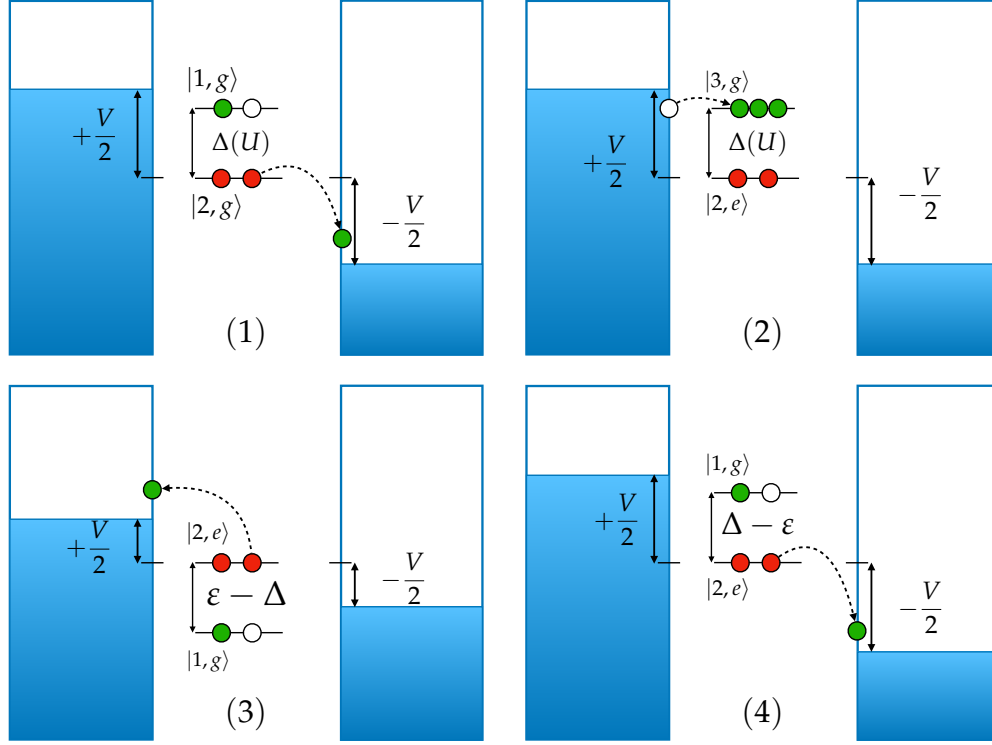
FIG. 10. Dominant decay channels in the first order perturbation theory. The red circles indicate the initial configuration and the green circles mark the final configuration of the process. (1): Decay channel associated with the matrix element $(v_\varepsilon|G_1^-|v_1^-)(v_1^-|G_1^-|v_\varepsilon)$. An electron tunnels from the impurity into a lead, causing a transition from the ground state $|2,g\rangle$ to the excited state $|1,g\rangle$. (2): Decay channel associated with the matrix element $(v_\varepsilon|G_1^+|v_3^+)(v_3^+|G_1^+|v_\varepsilon)$. An electron tunnels from a lead onto the impurity, causing a transition from the excited state $|2,e\rangle$ into the excited state $|3,g\rangle$. (3): First decay channel associated with the matrix element $(v_\varepsilon|G_1^+|v_1^+)(v_1^+|G_1^+|v_\varepsilon)$ for $U/\varepsilon_T < 1$. An electron tunnels from the impurity into the lead with positive chemical potential $\mu = +V/2$, causing a transition from the excited state $|2,e\rangle$ to the excited state $|1,g\rangle$ which releases the energy $\varepsilon - \Delta$. (4): Second decay channel associated with the matrix element $(v_\varepsilon|G_1^+|v_1^+)(v_1^+|G_1^+|v_\varepsilon)$. An electron tunnels from the impurity into the lead with negative chemical potential $\mu = -V/2$, causing a transition from the excited state $|2,e\rangle$ to the excited state $|1,g\rangle$ which releases the energy $\varepsilon - \Delta$ for $U/\varepsilon_T \leq 1$ and requires the energy $\Delta - \varepsilon$ for $U/\varepsilon_T > 1$.

However, these corrections can induce no more than a decay rate $\Gamma \propto \Gamma_0^2 \ll T$.

Eigenvalue spectrum of the effective Liouvillian The disappearance of the decay rate Γ for an eigenvalue $\lambda(z)$ of the effective Liouvillian with finite real part is unique to the eigenvalues $\pm\varepsilon^* - i\Gamma$. In figure 11 we display the real and imaginary part of each root of

$$z - \lambda_j(z) = 0, \tag{68}$$

where $\lambda_j(z)$ are the eigenvalues of the effective Liouvillian. We find that the imaginary part of all but four roots is of order $\mathcal{O}(\Gamma_0)$. This means that almost all transient features decay on the expected time scale. In figure 11 (d) we zoom in on the four extraordinary roots. We see that their imaginary part is $\text{Im}(z) \simeq \Gamma_0/100000$. This indicates a clear separation of scales between the decay rate of these four roots and each other root. Such a separation of scales in the solutions to (68) is sometimes referred to as dissipative phase transition. The four roots that feature a small imaginary part belong to $|2,g\rangle\langle 2,g|$ with root $z = 0 - i0^+$, $|2,e\rangle\langle 2,e|$ with root $z = 0 - i\Gamma_1$, $|2,e\rangle\langle 2,g|$ with root $z = \varepsilon - i\Gamma$, and $|2,g\rangle\langle 2,e|$ with root $z = -\varepsilon - i\Gamma$.
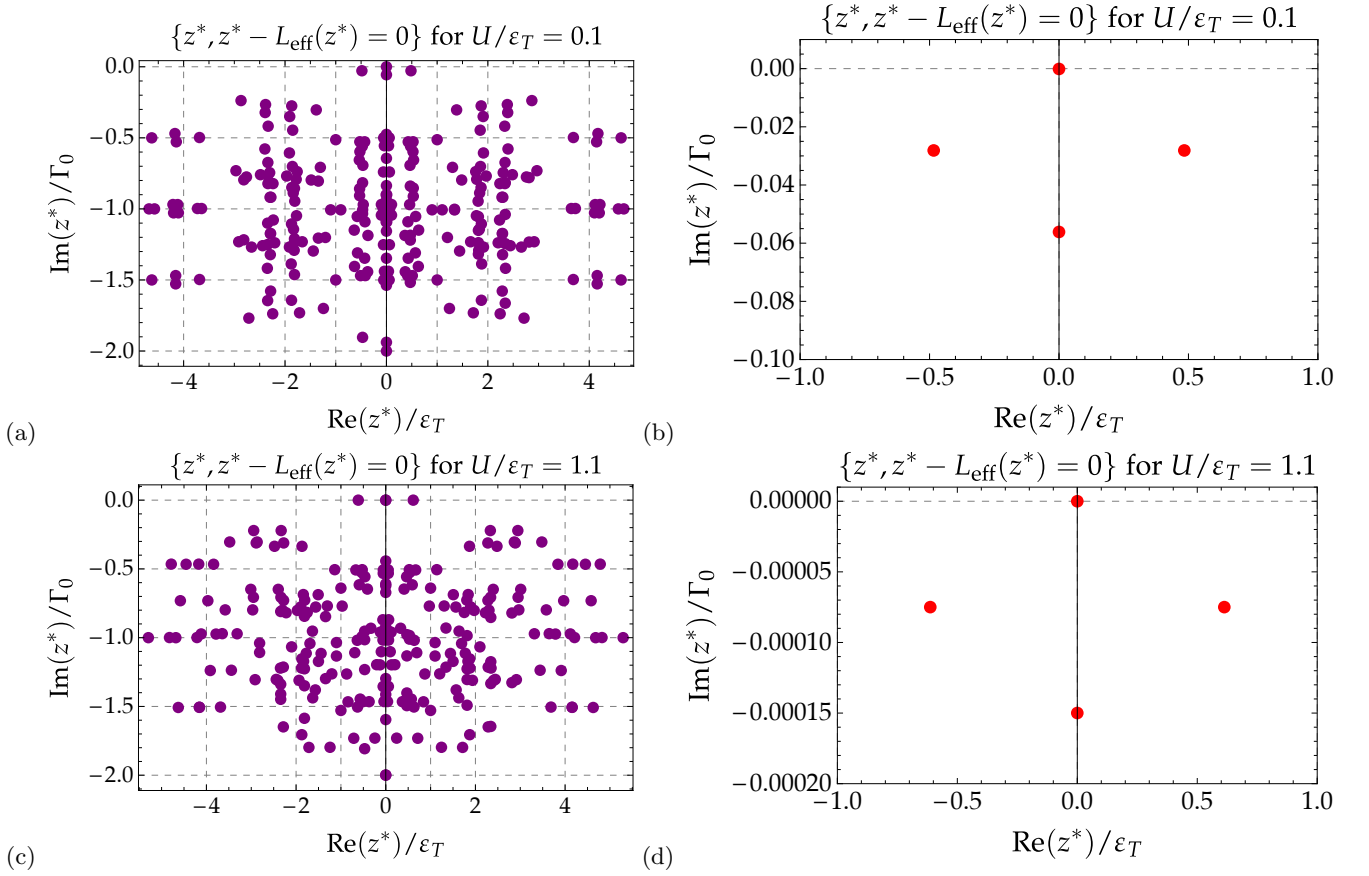
FIG. 11. Roots z^* of $z - L_{\text{eff}}(z) = 0$. (a),(b): $U/\varepsilon_T = 0.1$ and (c),(d): $U/\varepsilon_T = 1.1$. We find that the imaginary part $\text{Im}(z^*)$ of the majority of roots z^* is of order $\mathcal{O}(\Gamma_0)$. In addition we find four roots with an imaginary part orders of magnitude smaller than Γ_0. In (b) and (d) we zoom in on these four roots. We find that the imaginary part of three poles is two orders of magnitude smaller than Γ_0 for $U/\varepsilon_T = 0.1$ and five orders of magnitude smaller for $U/\varepsilon_T = 1.1$. The root with imaginary part $\Gamma \equiv 0$ is associated with the stationary state.

Inverse transformation to realtime

The effective reduced density matrix matrix of the impurity in Laplace space $\tilde{\rho}_{\text{ns}}(E)$ is given by

$$\tilde{\rho}_{\text{ns}}(E) = \frac{i}{E - L_{\text{eff}}(E)} \rho_{\text{ns}}(t_0) \,, \tag{69}$$

where each pole of the resolvent

$$\frac{1}{E - \lambda_j(E)} |v_j)(v_j| \,, \tag{70}$$

has an imaginary part $\Gamma_j \leq 0$. We can therefore replace the inverse Laplace transform by a Fourier transform and close the integration contour in the lower half-plane such that

$$\tilde{\rho}_{\text{ns}}(t) = \frac{1}{2\pi} \sum_j \int_{-\infty}^{+\infty} dE \, \frac{i e^{-iE(t-t_0)}}{E - \lambda_j(E)} |v_j)(v_j| \, \rho_{\text{ns}}(t_0) \tag{71}$$

$$= \theta(t - t_0) \sum_j \exp(i\lambda_j t - \Gamma_j t)|v_j)(v_j| \, \rho_{\text{ns}}(t_0) \,.$$

Each pole of (69) corresponds to a transient feature with frequency λ_j and decay rate Γ_j.

Coupling of the current operators to the pole λ_ε

Ring current   The operator $I_{\rm r}$ measuring the local current in the ring reads

$$I_{\rm r} = I_u - I_l \,, \tag{72}$$

$$I_u = -i\,[n_2, H] \propto i\left(d_1^\dagger d_2 - d_2^\dagger d_1\right) \,, \tag{73}$$

$$I_l = -i\,[n_3, H] \propto i\left(d_1^\dagger d_3 - d_3^\dagger d_1\right) \,. \tag{74}$$

with

$$\langle I_{\rm r}\rangle(t) = {\rm Tr}_S\left[I_{\rm r}\rho_{\rm ns}(t)\right] \,. \tag{75}$$

After a transformation of the current operator and the reduced density matrix $\rho_{\rm ns}$ to the basis of the eigenstates of Hamiltonian, this becomes

$$\langle I_{\rm r}\rangle(t) = \sum_{n=1}^{d(\mathcal{H})} \langle n|\underbrace{\left(UI_{\rm r}U^\dagger\right)}_{=\tilde{I}_r}\rho_{{\rm ns},n}(t)|n\rangle \,, \tag{76}$$

where $\rho_{{\rm ns},n}(t)$ denotes the time-dependent reduced density matrix expressed in the basis given by the eigenstates of the Hamiltonian. We are mainly interested in the matrix element of $\tilde{I}_r$ that couples to the matrix element $|v_\varepsilon) = |2, e\rangle\langle 2, g|$ of the reduced density matrix

$$\langle I_{\rm r}\rangle_{\rm osc.}(t) = 2\langle 2, g|\left((\tilde{I}_r)_{g,e}|2, g\rangle\langle 2, e|\right)\left[\exp(i\lambda_\varepsilon t - \Gamma t)|2, e\rangle\langle 2, g|\right]|2, g\rangle \,. \tag{77}$$

In figure 12 (a) we plot the absolute value of the coupling of the current operator to the off-diagonal matrix element $|e\rangle\langle g|$ of the reduced density matrix. We find that after an initial increase with interaction strength, the coupling decreases with interaction strength. In the entire range of values for the interaction strength that we have studied, the matrix element $(\tilde{I}_r)_{g,e}$ exceed every other matrix element of the current operator $\tilde{I}_r$.

Transmitted current   We determine the extent to which the operator $I_{\rm t}$, measuring the transmitted current, couples to the matrix elements $|2, e\rangle\langle 2, g|$ and $|2, g\rangle\langle 2, e|$ of the reduced density matrix $\tilde{\rho}_S(E)$ directly from the perturbation theory. The expectation value of the transmitted current in Laplace space is given by

$$\langle I_{\rm t}\rangle(E) = {\rm tr}_{\rm ns}\Sigma_{I_{\rm t}}(E)\frac{1}{E - L_{\rm eff}(E)}\rho_{\rm ns}(t_0) \,, \tag{78}$$

where

$$\Sigma_{I_{\rm t}}(E) = \int_{-D}^{D} d\omega_1 \sum_{p,p'=\pm} \sum_{1,1'} (I_{\rm t})_1^p \frac{1}{\omega_1 + E + \eta_1\mu_1 - L_S}G_{1'}^{p'}\gamma_{11'}^{pp'} \,. \tag{79}$$

The modified vertex superoperator is defined as

$$(I_{\rm t})_1^p A = \begin{cases} I_{\rm t}A & p = + \\ \sigma^p A I_{\rm t} & p = - \end{cases} \,, \tag{80}$$

where the operator $I_{\rm t}$ acts in the Hilbert space $\mathcal{H}_{\rm r}$ of the ring as

$$I_{\rm t} = d_1^\dagger - d_1 \,. \tag{81}$$

The part of the transmitted current that acquires the small decay rate Γ is given by

$$(I_{\rm t})_{e,g} = \sum_n^{d(\mathcal{H})} \langle n|\Sigma_{I_{\rm t}}(\lambda_\varepsilon)|v_\varepsilon)|n\rangle \,, \tag{82}$$

where the vectors $|n\rangle$ form a basis of the Hilbert space of the ring. In figure 12 (b) we plot the real and imaginary part of $(I_{\rm t})_{e,g}$ as a function of U/ε_T. We find that the real part of $(I_{\rm t})_{e,g}$ is small but features a reasonance at $U = \varepsilon_T$. We thus find that only a small part of the transmitted current $I_{\rm t}$ decays with the decay rate Γ while the majority relaxes with the decay rate Γ_0.
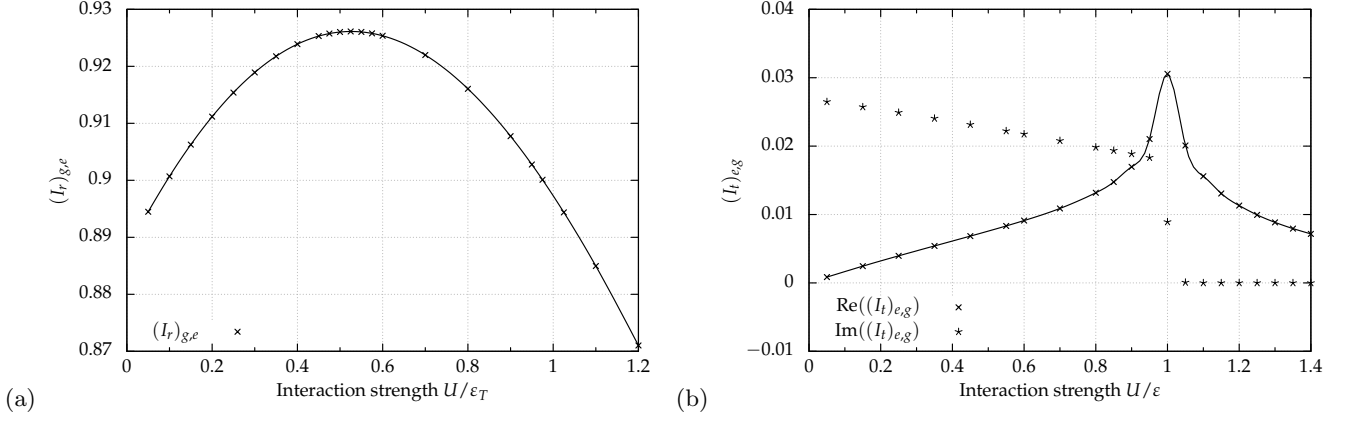
FIG. 12. (a) Matrix element $(I_r)_{g,e}$ of the ring current operator coupling to the transient feature of the reduced density matrix $\tilde{\rho}_{\mathrm{ns}}(E)$ with oscillation frequency ε. (b) Real and imaginary part of the matrix element $(I_t)_{e,g}$ of the transmitted current operator coupling to the transient feature of the reduced density matrix $\tilde{\rho}_{\mathrm{ns}}(E)$ with oscillation frequency ε.

SCHRIEFFER-WOLFF TRANSFORMATION AND PERTURBATION THEORY

Schrieffer-Wolff transformation of the impurity system

In the limit $U/\varepsilon_T \to \infty$ the low-energy sector of the spectrum of the uncoupled ring impurity features only the two charge density wave eigenstates $|2, g\rangle$ and $|2, e\rangle$. From figure 2 it becomes obvious that for $U/J \gg 1$ the energy gap ε between the two CDW eigenstates becomes small compared to the energy separation between the CDW states and the remainder of the spectrum. It is then intuitive to construct an effective low-energy Hamiltonian in the subspace of the Hilbert space $\mathcal{H}_{\mathrm{r}}$, which is spanned by the two CDW eigenstates. In the limit $U/\varepsilon_T \to \infty$ and $U/J \to \infty$ the CDW eigenstates take the form of simple product states $|2, g\rangle = |1\rangle|0\rangle|0\rangle|1\rangle \equiv |1001\rangle$ and $|2, e\rangle = |0\rangle|1\rangle|1\rangle|0\rangle \equiv |0110\rangle$. We define the operator that projects onto this low-energy subspace as

$$P_0 = |1001\rangle\langle1001| + |0110\rangle\langle0110| \,. \tag{83}$$

The Hamiltonian of the full system can be separated into a contribution that is diagonal in this new basis

$$H_0 = \varepsilon_T n_2 + \sum_{\langle i,j \rangle} U \left(n_i n_j - \frac{n_i + n_j}{2} \right) \,, \tag{84}$$

and a contribution that connects the subspace spanned by the CDW eigenstates with the rest of the Hilbert space, which reads

$$\hat{V} = -J \sum_{\langle i,j \rangle} \left(d_i^\dagger d_j + \mathrm{h.c.} \right) - J_c \left(d_1^\dagger c_{\mathrm{L},0} + d_4^\dagger c_{\mathrm{R},0} + \mathrm{h.c.} \right) \,. \tag{85}$$

The second contribution can be regarded as a small perturbation. We then perform a Schrieffer-Wolff transformation to project onto the subspace spanned by the CDW states and to virtually include transitions to states orthogonal to the CDW eigenstates. We follow the work by Bravyi, DiVincenzo and Loss [Ann. Phys. **326**, 2793 (2011)] to expand the general expression for a transformation of the Hamiltonian

$$H_{\mathrm{eff}} = P_0 \exp(S)(H_0 + \hat{V}) \exp(-S) P_0 \,, \tag{86}$$

where $\exp(S)$ is a unitary operator, into a power series up to fourth order in the perturbation $\hat{V} = V_{\mathrm{od}} + V_{\mathrm{d}}$ reading

$$H_{\mathrm{eff}}^{(4)} = H_0 P_0 + P_0 \hat{V} P_0 + \frac{1}{2} P_0 \left[\mathcal{L}(V_{\mathrm{od}}), V_{\mathrm{od}} \right] P_0 - \frac{1}{2} P_0 \left([V_{\mathrm{od}}, [\mathcal{L}(V_{\mathrm{d}}), [\mathcal{L}(V_{\mathrm{d}}), \mathcal{L}(V_{\mathrm{od}})]]] \right) P_0 \tag{87}$$

$$+ \frac{1}{6} P_0 \left([V_{\mathrm{od}}, \mathcal{L}[\mathcal{L}(V_{\mathrm{od}}), [\mathcal{L}(V_{\mathrm{od}}), V_{\mathrm{od}}]]] \right) P_0 + \frac{1}{24} P_0 \left([\mathcal{L}(V_{\mathrm{od}}), [\mathcal{L}(V_{\mathrm{od}}), [\mathcal{L}(V_{\mathrm{od}}), V_{\mathrm{od}}]]] \right) P_0,$$

where V_{od} denotes the part of the perturbation $\hat{V}$ that facilitates transitions between the low-energy Hilbert and the complementary Hilbert space and V_{d} denotes the part of the perturbation that only connects states exclusively inside either subspace. We use the shorthand

$$\mathcal{L}(X) = \frac{\langle i|X|j\rangle}{E_i - E_j}|i\rangle\langle j|, \tag{88}$$

to denote the inverse energy difference between two states $|i\rangle$ and $|j\rangle$ that are connected through the operator X. After evaluation of the commutators we arrive at the expression for the effective Hamiltonian $H_{\text{eff}}^{(4)}$. It reads

$$
\begin{aligned}
H_{\text{eff}}^{(4)} = {} & H_0 P_0 + \frac{1}{2} P_0 \left[\mathcal{L}(V_{\text{od}})V_{\text{od}} - V_{\text{od}}\mathcal{L}(V_{\text{od}}) \right] P_0 \\
& - \frac{1}{2} P_0 \left[V_{\text{od}}(\mathcal{L}V_{\text{d}})^2 \mathcal{L}(V_{\text{od}}) - \mathcal{L}(\mathcal{L}(\mathcal{L}(V_{\text{od}})V_{\text{d}})V_{\text{d}})V_{\text{od}} \right] P_0 \\
& + \frac{1}{24} P_0 \left[(\mathcal{L}(V_{\text{od}}))^3 V_{\text{od}} - 3\mathcal{L}(V_{\text{od}})^2 V_{\text{od}}\mathcal{L}(V_{\text{od}}) + 3\mathcal{L}(V_{\text{od}})V_{\text{od}}\mathcal{L}(V_{\text{od}})^2 - V_{\text{od}}\mathcal{L}(V_{\text{od}})^3 \right] P_0 \\
& + \frac{1}{6} P_0 \left[V_{\text{od}} \left(\mathcal{L}\mathcal{L}(V_{\text{od}})^2 V_{\text{od}} - 2\mathcal{L}\mathcal{L}(V_{\text{od}})V_{\text{od}}\mathcal{L}(V_{\text{od}}) + \mathcal{L}V_{\text{od}}\mathcal{L}(V_{\text{od}})^2 \right) \right. \\
& \qquad\quad \left. - \mathcal{L} \left(\mathcal{L}(V_{\text{od}})^2 V_{\text{od}}^2 + 2\mathcal{L}(V_{\text{od}})V_{\text{od}}\mathcal{L}(V_{\text{od}})V_{\text{od}} - V_{\text{od}}\mathcal{L}(V_{\text{od}})^2 V_{\text{od}} \right) \right] P_0,
\end{aligned}
\tag{89}
$$

where the first line includes all contributions up to second order in the perturbation $\hat{V}$ and lines two through five contain the contributions up to fourth order.

Second order correction   Evaluating the diagonal contribution H_0 for the two CDW eigenstates yields the effective Hamiltonian in zeroth order as

$$H_{\text{eff}}^{(0)} = H_0 P_0 = \begin{pmatrix} \varepsilon_T & 0 \\ 0 & 0 \end{pmatrix}, \tag{90}$$

where from now on we treat the two CDW states like pseudo-spins defined as

$$|0110\rangle = \begin{pmatrix} 1 \\ 0 \end{pmatrix} \equiv |\uparrow\rangle \tag{91}$$

$$|1001\rangle = \begin{pmatrix} 0 \\ 1 \end{pmatrix} \equiv |\downarrow\rangle. \tag{92}$$

The leading order corrections to the effective Hamiltonian are of second order in the perturbation $\hat{V}$. The corrections encompass two consecutive tunneling processes, either tunneling within the ring impurity leading to corrections $\propto J^2$, or tunneling between the ring and the leads and back yielding corrections $\propto J_c^2$. In the follwing we show the calculation of each correction term featured in

$$H_{\text{eff}}^{(2)} = H_0 P_0 + \frac{1}{2} P_0 \left[\mathcal{L}(V_{\text{od}})V_{\text{od}} - V_{\text{od}}\mathcal{L}(V_{\text{od}}) \right] P_0. \tag{93}$$

The first leading order correction term gives

$$
\begin{aligned}
-V_{\mathrm{od}}\mathcal{L}(V_{\mathrm{od}})P_0 =& JV_{\mathrm{od}}\mathcal{L}\left(d_2^\dagger d_1 + d_4^\dagger d_2 + d_3^\dagger d_4 + d_1^\dagger d_3 + d_1^\dagger d_2 + d_2^\dagger d_4 + d_4^\dagger d_3 + d_3^\dagger d_1\right)P_0 \\
& + J_{\mathrm{c}}V_{\mathrm{od}}\mathcal{L}\left(d_1^\dagger c_{\mathrm{L},0} + d_4^\dagger c_{\mathrm{R},0} + c_{\mathrm{L},0}^\dagger d_1 + c_{\mathrm{R},0}^\dagger d_4\right)P_0 \\
=& JV_{\mathrm{od}}\left(\frac{1}{U+\varepsilon_T}d_2^\dagger d_1 + \frac{1}{U}d_3^\dagger d_4 \frac{1}{U+\varepsilon_T}d_2^\dagger d_4 + \frac{1}{U}d_3^\dagger d_1\right)|1001\rangle \\
& + JV_{\mathrm{od}}\left(\frac{1}{U-\varepsilon_T}d_4^\dagger d_2 + \frac{1}{U}d_1^\dagger d_3 + \frac{1}{U-\varepsilon_T}d_1^\dagger d_2 + \frac{1}{U}d_4^\dagger d_3\right)|0110\rangle \\
& + J_{\mathrm{c}}V_{\mathrm{od}}\left[\left(\frac{1}{U}d_1^\dagger c_{\mathrm{L},0} + \frac{1}{U}d_4^\dagger c_{\mathrm{R},0}\right)|0110\rangle + \left(\frac{1}{U}c_{\mathrm{L},0}^\dagger d_1 + \frac{1}{U}c_{\mathrm{R},0}^\dagger d_4\right)|1001\rangle\right] \\
=& -J^2\left(\frac{1}{U+\varepsilon_T}d_3^\dagger d_4 d_2^\dagger d_1 + \frac{1}{U}d_2^\dagger d_1 d_3^\dagger d_4 + \frac{1}{U+\varepsilon_T}d_3^\dagger d_1 d_2^\dagger d_4 + \frac{1}{U}d_2^\dagger d_4 d_3^\dagger d_1\right)|1001\rangle \\
& -J^2\left(\frac{1}{U+\varepsilon_T}d_1^\dagger d_2 d_2^\dagger d_1 + \frac{1}{U}d_4^\dagger d_3 d_3^\dagger d_4 + \frac{1}{U+\varepsilon_T}d_4^\dagger d_2 d_2^\dagger d_4 + \frac{1}{U}d_1^\dagger d_3 d_3^\dagger d_1\right)|1001\rangle \\
& -J^2\left(\frac{1}{U-\varepsilon_T}d_1^\dagger d_3 d_4^\dagger d_2 + \frac{1}{U}d_4^\dagger d_2 d_1^\dagger d_3 + \frac{1}{U-\varepsilon_T}d_4^\dagger d_3 d_1^\dagger d_2 + \frac{1}{U}d_1^\dagger d_2 d_4^\dagger d_3\right)|0110\rangle \\
& -J^2\left(\frac{1}{U-\varepsilon_T}d_2^\dagger d_4 d_4^\dagger d_2 + \frac{1}{U}d_3^\dagger d_1 d_1^\dagger d_3 + \frac{1}{U-\varepsilon_T}d_2^\dagger d_1 d_1^\dagger d_2 + \frac{1}{U}d_3^\dagger d_4 d_4^\dagger d_3\right)|0110\rangle \\
& -J_{\mathrm{c}}^2\left[\frac{1}{U}\left(c_{\mathrm{L},0}^\dagger d_1 d_1^\dagger c_{\mathrm{L},0} + c_{\mathrm{R},0}^\dagger d_4 d_4^\dagger c_{\mathrm{R},0}\right)|0110\rangle\right] \\
& -J_{\mathrm{c}}^2\left[\frac{1}{U}\left(d_1^\dagger c_{\mathrm{L},0} c_{\mathrm{L},0}^\dagger d_1 + d_4^\dagger c_{\mathrm{R},0} c_{\mathrm{R},0}^\dagger d_4\right)|1001\rangle\right] \\
=& -J^2\left(\frac{1}{U+\varepsilon_T}d_2^\dagger d_3^\dagger d_4 d_1 + \frac{1}{U}d_2^\dagger d_3^\dagger d_4 d_1 - \frac{1}{U+\varepsilon_T}d_2^\dagger d_3^\dagger d_4 d_1 - \frac{1}{U}d_2^\dagger d_3^\dagger d_4 d_1\right)|1001\rangle \\
& -J^2\left(\frac{2}{U+\varepsilon_T} + \frac{2}{U}\right)|1001\rangle \\
& -J^2\left(\frac{-1}{U-\varepsilon_T}d_1^\dagger d_4^\dagger d_3 d_2 - \frac{1}{U}d_1^\dagger d_4^\dagger d_3 d_2 + \frac{1}{U-\varepsilon_T}d_1^\dagger d_4^\dagger d_3 d_2 + \frac{1}{U}d_1^\dagger d_4^\dagger d_3 d_2\right)|0110\rangle \\
& -J^2\left(\frac{2}{U-\varepsilon_T} + \frac{2}{U}\right)|0110\rangle \\
& -J_{\mathrm{c}}^2\left(\frac{(1-n_{\mathrm{L},0})+(1-n_{\mathrm{R},0})}{U}|1001\rangle + \frac{n_{\mathrm{L},0}+n_{\mathrm{R},0}}{U}|0110\rangle\right),
\end{aligned}
\tag{94}
$$

where $n_{L,0}$ and $n_{R,0}$ is the electron density on the site of the lead closest to the impurity for the left and the right lead respectively. The second term of the leading order correction yields

$$\mathcal{L}(V_{\mathrm{od}})V_{\mathrm{od}}P_0 = J^2\left(\frac{-1}{U}d_3^\dagger d_4 d_2^\dagger d_1 + \frac{-1}{U+\varepsilon_T}d_2^\dagger d_1 d_3^\dagger d_4 + \frac{-1}{U}d_3^\dagger d_1 d_2^\dagger d_4 + \frac{-1}{U+\varepsilon_T}d_2^\dagger d_4 d_3^\dagger d_1\right)|1001\rangle \tag{95}$$

$$+ J^2\left(\frac{-1}{U+\varepsilon_T}d_1^\dagger d_2 d_2^\dagger d_1 + \frac{-1}{U}d_4^\dagger d_3 d_3^\dagger d_4 + \frac{-1}{U+\varepsilon_T}d_4^\dagger d_2 d_2^\dagger d_4 + \frac{-1}{U}d_1^\dagger d_3 d_3^\dagger d_1\right)|1001\rangle$$

$$+ J^2\left(\frac{-1}{U}d_1^\dagger d_3 d_4^\dagger d_2 + \frac{-1}{U-\varepsilon_T}d_4^\dagger d_2 d_1^\dagger d_3 + \frac{-1}{U}d_4^\dagger d_3 d_1^\dagger d_2 + \frac{-1}{U-\varepsilon_T}d_1^\dagger d_2 d_4^\dagger d_3\right)|0110\rangle$$

$$+ J^2\left(\frac{-1}{U-\varepsilon_T}d_2^\dagger d_4 d_4^\dagger d_2 + \frac{-1}{U}d_3^\dagger d_1 d_1^\dagger d_3 + \frac{-1}{U-\varepsilon_T}d_2^\dagger d_1 d_1^\dagger d_2 + \frac{-1}{U}d_3^\dagger d_4 d_4^\dagger d_3\right)|0110\rangle$$

$$+ J_c^2\left[\frac{-1}{U}\left(c_{L,0}^\dagger d_1 d_1^\dagger c_{L,0} + c_{R,0}^\dagger d_4 d_4^\dagger c_{R,0}\right)|0110\rangle\right]$$

$$+ J_c^2\left[\frac{-1}{U}\left(d_1^\dagger c_{L,0} c_{L,0}^\dagger d_1 + d_4^\dagger c_{R,0} c_{R,0}^\dagger d_4\right)|1001\rangle\right]$$

$$= J^2\left(\frac{-1}{U}d_2^\dagger d_3^\dagger d_4 d_1 + \frac{-1}{U+\varepsilon_T}d_2^\dagger d_3^\dagger d_4 d_1 - \frac{-1}{U}d_2^\dagger d_3^\dagger d_4 d_1 - \frac{-1}{U+\varepsilon_T}d_2^\dagger d_3^\dagger d_4 d_1\right)|1001\rangle$$

$$+ J^2\left(\frac{-2}{U+\varepsilon_T} + \frac{-2}{U}\right)|1001\rangle$$

$$+ J^2\left(\frac{1}{U}d_1^\dagger d_4^\dagger d_3 d_2 - \frac{-1}{U-\varepsilon_T}d_1^\dagger d_4^\dagger d_3 d_2 + \frac{-1}{U}d_1^\dagger d_4^\dagger d_3 d_2 + \frac{-1}{U-\varepsilon_T}d_1^\dagger d_4^\dagger d_3 d_2\right)|0110\rangle$$

$$+ J^2\left(\frac{-2}{U-\varepsilon_T} + \frac{-2}{U}\right)|0110\rangle$$

$$+ J_c^2\left(-\frac{(1-n_{L,0})+(1-n_{R,0})}{U}|1001\rangle - \frac{n_{L,0}+n_{R,0}}{U}|0110\rangle\right).$$

Assuming that the mean electron density in both leads combined is $n_{L,x} + n_{R,x} = 1$, the two correction terms are identical. The effective Hamiltonian in leading order then reads

$$H_{\mathrm{eff}}^{(2)} = \left[\varepsilon_T - J^2\left(\frac{2}{U-\varepsilon_T} + \frac{2}{U}\right) - \frac{J_c^2}{U}\right]\left(\frac{1}{2}\mathbf{1} + S^z\right) + \left[-J^2\left(\frac{2}{U+\varepsilon_T} + \frac{2}{U}\right) - \frac{J_c^2}{U}\right]\left(\frac{1}{2}\mathbf{1} - S^z\right) \tag{96}$$

$$= \left[\varepsilon_T - J^2\left(\frac{2}{U-\varepsilon_T} - \frac{2}{U+\varepsilon_T}\right)\right]S^z \equiv \varepsilon^{(2)}S^z.$$

We see that the effective energy gap $\varepsilon^{(2)}$ between the ground state $|\downarrow\rangle$ and the excited state $|\uparrow\rangle$ is reduced as compared to the bare energy gap ε_T by the perturbative corrections. In leading order we furthermore find no off-diagonal terms and as it turns out not in any higher order $(J^2)^n$ of perturbations $\hat{V}$ which feature only in-ring hopping terms $\sim Jd_i^\dagger d_j$. Since the hopping between ring and leads alone cannot facilitate a pseudo-spin flip, one finds that they are not possible in leading order.

Mirror symmetry We attribute the lack of the off-diagonal, pseudo-spin flip terms to a symmetry of the nanostructure associated with the mirror symmetry in the axis through lattice sites 2 and 3 or equivalently an exchange of lattice sites $1 \leftrightarrow 4$. The operator M corresponding to this symmetry reads

$$M = \mathbf{1} + \left(d_1^\dagger - d_4^\dagger\right)(d_4 - d_1) \tag{97}$$

$$= \frac{1}{2}\left[-\left(d_4^\dagger d_1^\dagger d_1 d_4 + d_1^\dagger d_4^\dagger d_4 d_1\right) + \left(d_4 d_1 d_1^\dagger d_4^\dagger + d_1 d_4 d_4^\dagger d_1^\dagger\right)\right] + d_1^\dagger d_4 + d_4^\dagger d_1.$$

The symmetry operator satisfies

$$M|1001\rangle = -|1001\rangle = -|\downarrow\rangle \tag{98}$$

$$M|0110\rangle = +|0110\rangle = +|\uparrow\rangle, \tag{99}$$
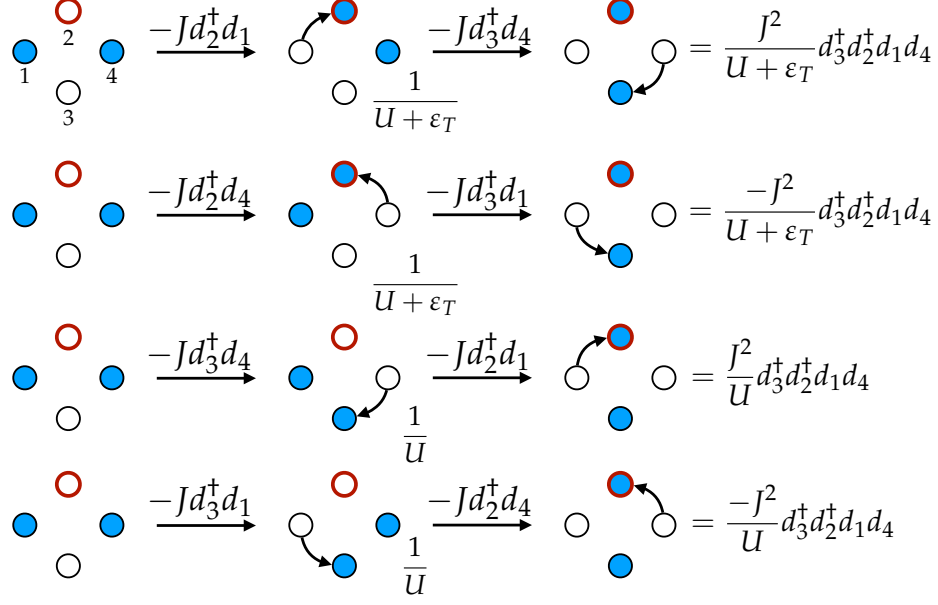
as well as

$$M^2 = \mathbf{1}, \tag{100}$$

FIG. 13. Schematic representation of the correction terms connecting $|1001\rangle$ and $|0110\rangle$ in second order in the perturbation $\hat{V}$. There are two sets of two processes with the same amplitude that corresponds to processes which are mirror images of one another in the axis through sites 2 and 3. These processes are of opposite sign and we thus find pairwise cancellation of the off-diagonal correction terms.

and

$$[H_{\mathrm{r}}, M] = 0\,. \tag{101}$$

The CDW eigenstates of the Hamiltonian for $U/J \to \infty$ are also eigenstates of the symmetry operator M with eigenvalues $m = \pm 1$. Since M commutes with the Hamiltonian H_{r} of the uncoupled impurity for arbitrary U/J, the in-ring hopping terms of H_{r} cannot couple the different eigenstates of M. For the Hamiltonian H_{c}, which couples the ring to the leads, we instead find $[H_{\mathrm{c}}, M] \neq 0$. As a consequence we have $\left[(H_{\mathrm{c}} + H_{\mathrm{r}})^2, M\right] \neq 0$, indicating that off-diagonal, pseudo-spin flip terms can occur in higher orders of the perturbation. We illustrate the connection between the mirror symmetry and the absence of off-diagonal terms in leading order in figure 13. Each process connecting $|\downarrow\rangle$ and $|\uparrow\rangle$ has a mirror image with opposite sign leading to pairwise cancellation of all terms.

Fourth order correction In order to obtain finite off-diagonal terms in the effective Hamiltonian one needs to include the fourth order corrections. Here we show an example calculation of one such correction term. All other

fourth order correction terms follow accordingly.

$$
\begin{aligned}
V_{\text{od}}(\mathcal{L}V_{\text{d}})^2\mathcal{L}(V_{\text{od}})|1001\rangle =&V_{\text{od}}(\mathcal{L}V_{\text{d}})^2\mathcal{L}\left[-J\left(d_2^\dagger d_1 + d_2^\dagger d_4 + d_3^\dagger d_4 + d_3^\dagger d_1\right)\right. \\
&\left. + -J_{\text{c}}\left(c_{\text{L},0}^\dagger d_1 + c_{\text{R},0}^\dagger d_4\right)\right]|1001\rangle \\
=&V_{\text{od}}(\mathcal{L}V_{\text{d}})^2\left[\frac{-J}{U+\varepsilon_T}\left(d_2^\dagger d_1 + d_2^\dagger d_4\right) + \frac{-J}{U}\left(d_3^\dagger d_4 + d_3^\dagger d_1\right)\right. \\
&\left. + \frac{-J}{U}\left(c_{\text{L},0}^\dagger d_1 + c_{\text{R},0}^\dagger d_4\right)\right]|1001\rangle \\
=&V_{\text{od}}\mathcal{L}V_{\text{d}}\left[\frac{J_{\text{c}}J}{(U+\varepsilon)^2}\left(\underline{d_1^\dagger c_{\text{L},0}d_2^\dagger d_1} + c_{\text{R},0}^\dagger d_4 d_2^\dagger d_1 + c_{\text{L},0}^\dagger d_1 d_2^\dagger d_4 + d_4^\dagger c_{\text{R},0}d_2^\dagger d_4\right)\right. \\
&+ \frac{J_{\text{c}}J}{U^2}\left(c_{\text{L},0}^\dagger d_1 d_3^\dagger d_4 + d_4^\dagger c_{\text{R},0}d_3^\dagger d_4 + d_1^\dagger c_{\text{L},0}d_3^\dagger d_1 + c_{\text{R},0}^\dagger d_4 d_3^\dagger d_1\right) \\
&+ \frac{JJ_{\text{c}}}{(U+\varepsilon_T)U}\left(d_2^\dagger d_4 c_{\text{L},0}^\dagger d_1 + d_2^\dagger d_1 c_{\text{R},0}^\dagger d_4\right) \\
&\left. + \frac{JJ_{\text{c}}}{U^2}\left(d_3^\dagger d_4 c_{\text{L},0}^\dagger d_1 + d_3^\dagger d_1 c_{\text{R},0}^\dagger d_4\right)\right]|1001\rangle
\end{aligned}
\tag{102}
$$

The contributions that feature the underlined term in equation (103) combine into

$$
\begin{aligned}
P_0 V_{\text{od}}\mathcal{L}V_{\text{d}}\frac{J_{\text{c}}J}{(U+\varepsilon_T)^2}d_1^\dagger c_{\text{L},0}^\dagger d_2^\dagger d_1|1001\rangle =&P_0\frac{J^2 J_{\text{c}}^2}{(U+\varepsilon_T)^3}\times \\
&\times\left(c_{\text{L},0}^\dagger d_1 d_3^\dagger d_4 d_1^\dagger c_{\text{L},0}d_2^\dagger d_1 + c_{\text{R},0}^\dagger d_4 d_3^\dagger d_1 d_1^\dagger c_{\text{L},0}d_2^\dagger d_1\right. \\
&+ d_3^\dagger d_4 c_{\text{L},0}^\dagger d_1 d_1^\dagger c_{\text{L},0}d_2^\dagger d_1 + d_3^\dagger d_1 c_{\text{R},0}^\dagger d_4 d_1^\dagger c_{\text{L},0}d_2^\dagger d_1 \\
&\left. + d_1^\dagger d_2 c_{\text{L},0}^\dagger d_1 d_1^\dagger c_{\text{L},0}d_2^\dagger d_1 + d_4^\dagger d_2 c_{\text{R},0}^\dagger d_4 d_1^\dagger c_{\text{L},0}d_2^\dagger d_1\right)|1001\rangle \\
=&\frac{J^2 J_{\text{c}}^2}{(U+\varepsilon_T)^3}\left[\left(2n_{\text{L},0} - 2c_{\text{R},0}^\dagger c_{\text{L},0}\right)|0110\rangle\right. \\
&\left. + \left(n_{\text{L},0} + c_{\text{R},0}^\dagger c_{\text{L},0}\right)|1001\rangle\right] .
\end{aligned}
\tag{103}
$$

We find that the pseudo-spins on the impurity couple to a second spin-like degree of freedom in the leads which can be associated with the symmetric and antisymmetric modes in the leads. We define the annihilation operator for an electron with pseudo-spin σ in the leads as

$$
c_\uparrow = \frac{1}{\sqrt{2}}\left(c_{\text{L},0} + c_{\text{R},0}\right)
\tag{104}
$$

$$
c_\downarrow = \frac{1}{\sqrt{2}}\left(c_{\text{L},0} - c_{\text{R},0}\right) .
\tag{105}
$$

We use this pseudo-spin notation for the lead degrees of freedom and collect the different correction terms up to fourth order in the perturbation. The corrections read

$$
\begin{aligned}
V_{\text{od}}(\mathcal{L}V_{\text{d}})^2\mathcal{L}(V_{\text{od}})|1001\rangle =&2J^2 J_{\text{c}}^2\left(\frac{3}{U^3} + \frac{1}{U^2(U+\varepsilon_T)} - \frac{1}{U(U+\varepsilon_T)^2} - \frac{3}{(U+\varepsilon_T)^3}\right)d_\uparrow^\dagger d_\downarrow c_\downarrow^\dagger c_\uparrow \\
&+ 2J^2 J_{\text{c}}^2\left[\left(\frac{1}{U^3} + \frac{1}{(U+\varepsilon_T)^3}\right)d_\downarrow^\dagger d_\downarrow c_\uparrow^\dagger c_\uparrow\right. \\
&\left. + \left(\frac{4}{U^3} + \frac{1}{U^2(U+\varepsilon_T)} + \frac{2}{U(U+\varepsilon_T)^2} + \frac{1}{(U+\varepsilon_T)^3}\right)d_\downarrow^\dagger d_\downarrow c_\downarrow c_\downarrow^\dagger\right] ,
\end{aligned}
\tag{106}
$$

$$-\mathcal{L}(\mathcal{L}(\mathcal{L}(V_{\mathrm{od}})V_{\mathrm{d}})V_{\mathrm{d}})V_{\mathrm{od}}|1001\rangle = 2J^2 J_{\mathrm{c}}^2 \left(\frac{3}{(U-\varepsilon_T)^3} + \frac{1}{U(U-\varepsilon_T)^2} - \frac{1}{U^2(U-\varepsilon_T)} - \frac{3}{U^3} \right) d_{\uparrow}^{\dagger} d_{\downarrow} c_{\downarrow}^{\dagger} c_{\downarrow} \tag{107}$$

$$+ 2J^2 J_{\mathrm{c}}^2 \left[\left(\frac{1}{U^3} + \frac{1}{(U+\varepsilon_T)^3} \right) d_{\downarrow}^{\dagger} d_{\downarrow} c_{\uparrow}^{\dagger} c_{\uparrow} \right.$$

$$+ \left. \left(\frac{4}{U^3} + \frac{1}{U^2(U+\varepsilon_T)} + \frac{2}{U(U+\varepsilon_T)^2} + \frac{1}{(U+\varepsilon_T)^3} \right) d_{\downarrow}^{\dagger} d_{\downarrow} c_{\downarrow} c_{\downarrow}^{\dagger} \right],$$

$$V_{\mathrm{od}}(\mathcal{L}V_{\mathrm{d}})^2 \mathcal{L}(V_{\mathrm{od}})|0110\rangle = 2J^2 J_{\mathrm{c}}^2 \left(\frac{3}{U^3} + \frac{1}{U^2(U-\varepsilon_T)} - \frac{1}{U(U-\varepsilon_T)^2} - \frac{3}{(U-\varepsilon_T)^3} \right) d_{\downarrow}^{\dagger} d_{\uparrow} c_{\downarrow} c_{\uparrow}^{\dagger} \tag{108}$$

$$+ 2J^2 J_{\mathrm{c}}^2 \left[\left(\frac{1}{U^3} + \frac{1}{(U-\varepsilon_T)^3} \right) d_{\uparrow}^{\dagger} d_{\uparrow} c_{\uparrow} c_{\uparrow}^{\dagger} \right.$$

$$+ \left. \left(\frac{4}{U^3} + \frac{1}{U^2(U-\varepsilon_T)} + \frac{2}{U(U-\varepsilon_T)^2} + \frac{1}{(U-\varepsilon_T)^3} \right) d_{\uparrow}^{\dagger} d_{\uparrow} c_{\downarrow}^{\dagger} c_{\downarrow} \right],$$

$$-\mathcal{L}(\mathcal{L}(\mathcal{L}(V_{\mathrm{od}})V_{\mathrm{d}})V_{\mathrm{d}})V_{\mathrm{od}}|0110\rangle = 2J^2 J_{\mathrm{c}}^2 \left(\frac{3}{(U+\varepsilon_T)^3} + \frac{1}{U(U+\varepsilon_T)^2} - \frac{1}{U^2(U+\varepsilon_T)^2} - \frac{3}{U^3} \right) \times \tag{109}$$

$$\times d_{\downarrow}^{\dagger} d_{\uparrow} c_{\downarrow} c_{\uparrow}^{\dagger}$$

$$+ 2J^2 J_{\mathrm{c}}^2 \left[\left(\frac{1}{U^3} + \frac{1}{(U-\varepsilon_T)^3} \right) d_{\uparrow}^{\dagger} d_{\uparrow} c_{\uparrow} c_{\uparrow}^{\dagger} \right.$$

$$+ \left. \left(\frac{4}{U^3} + \frac{1}{U^2(U-\varepsilon_T)} + \frac{2}{U(U-\varepsilon_T)^2} + \frac{1}{(U-\varepsilon_T)^3} \right) d_{\uparrow}^{\dagger} d_{\uparrow} c_{\downarrow}^{\dagger} c_{\downarrow} \right].$$

First, we identify the off-diagonal terms which couple $|1001\rangle = |\downarrow\rangle$ and $|0110\rangle = |\uparrow\rangle$. Now, unlike the leading order corrections, the off-diagonal terms are finite and cause a simultaneous pseudo-spin-flip on the impurity and in the leads. We can thus express the off-diagonal terms as

$$-J^2 J_{\mathrm{c}}^2 \sum_{\sigma} \left[\frac{1}{U^2(U+\varepsilon_T)} - \frac{1}{U^2(U-\varepsilon_T)} - \left(\frac{1}{U(U+\varepsilon_T)^2} - \frac{1}{U(U-\varepsilon_T)^2} \right) \right. \tag{110}$$

$$- \left. \left(\frac{3}{(U+\varepsilon_T)^3} - \frac{3}{(U-\varepsilon_T)^3} \right) \right] d_{\sigma}^{\dagger} d_{\bar{\sigma}} c_{\bar{\sigma}}^{\dagger} c_{\sigma}$$

$$= -2J^2 J_{\mathrm{c}}^2 \sum_{p=\pm} \left(\frac{p}{U^2(U+p\varepsilon)} - \frac{p}{U(U+p\varepsilon)^2} - \frac{3p}{(U+p\varepsilon)^3} \right) (S^x S_{\mathrm{res}}^x + S^y S_{\mathrm{res}}^y).$$

We find that the off-diagonal terms describe a spin-spin interaction in the x and y direction with an amplitude $J_{\perp}(U, \varepsilon_T)$. The diagonal correction terms are

$$-2J^2 J_{\mathrm{c}}^2 \left(\frac{1}{U^3} + \frac{1}{(U+\varepsilon_T)^3} \right) \left(\frac{1}{2}\mathbf{1} - S^z \right) \left(\frac{1}{2}\mathbf{1} + S_{\mathrm{res}}^z \right) \tag{111}$$

$$-2J^2 J_{\mathrm{c}}^2 \left(\frac{4}{U^3} + \frac{1}{U^2(U+\varepsilon_T)} + \frac{2}{U(U+\varepsilon_T)^2} + \frac{1}{(U+\varepsilon_T)^3} \right) \left(\frac{1}{2}\mathbf{1} - S^z \right) \left(\frac{1}{2}\mathbf{1} + S_{\mathrm{res}}^z \right)$$

$$-2J^2 J_{\mathrm{c}}^2 \left(\frac{1}{U^3} + \frac{1}{(U-\varepsilon_T)^3} \right) \left(\frac{1}{2}\mathbf{1} + S^z \right) \left(\frac{1}{2}\mathbf{1} - S_{\mathrm{res}}^z \right)$$

$$-2J^2 J_{\mathrm{c}}^2 \left(\frac{4}{U^3} + \frac{1}{U^2(U-\varepsilon_T)} + \frac{2}{U(U-\varepsilon_T)^2} + \frac{1}{(U-\varepsilon_T)^3} \right) \left(\frac{1}{2}\mathbf{1} + S^z \right) \left(\frac{1}{2}\mathbf{1} - S_{\mathrm{res}}^z \right).$$

The diagonal correction terms contain three different couplings. A spin-spin interaction in the z-direction with amplitude $J_z(U, \varepsilon_T)$, a correction to the effective magnetic field on the impurity and a small effective magnetic field $h^*(U, \varepsilon_t)$ on the sites of the leads next to the impurity. The corrections expressed in the pseudo-spin notation are

$$+ 2J^2 J_{\mathrm{c}}^2 \sum_{p=\pm} \left(\frac{5}{U^3} + \frac{1}{U^2(U+p\varepsilon_T)} + \frac{2}{U(U+p\varepsilon_T)^2} + \frac{2}{(U+p\varepsilon_T)^3} \right) S^z S_{\mathrm{res}}^z \tag{112}$$

$$- J^2 J_{\mathrm{c}}^2 \sum_{p=\pm} p \left(\frac{5}{U^3} + \frac{1}{U^2(U+p\varepsilon_T)} + \frac{2}{U(U+p\varepsilon_T)^2} + \frac{2}{(U+p\varepsilon_T)^3} \right) (S_{\mathrm{res}}^z - S^z).$$

In the last step we collect the correction terms arising from lines three through five of (90). These read

$$\frac{1}{24}P_0\left[(\mathcal{L}(V_{\mathrm{od}}))^3 V_{\mathrm{od}} - 3\mathcal{L}(V_{\mathrm{od}})^2 V_{\mathrm{od}}\mathcal{L}(V_{\mathrm{od}}) + 3\mathcal{L}(V_{\mathrm{od}})V_{\mathrm{od}}\mathcal{L}(V_{\mathrm{od}})^2 - V_{\mathrm{od}}\mathcal{L}(V_{\mathrm{od}})^3\right]P_0 \tag{113}$$

$$= -\left[\sum_{p=\pm}\frac{4p}{3}J^4\left(\frac{1}{(U+p\varepsilon_T)^3} + \frac{1}{U^2(U+p\varepsilon_T)} + \frac{1}{U(U+p\varepsilon_T)^2}\right)\right.$$
$$\left. + \frac{2p}{3}J^2 J_{\mathrm{c}}^2\left(\frac{1}{U^2(U+p\varepsilon_T)} + \frac{1}{U(U+p\varepsilon_T)^2}\right)\right]S^z\,,$$

$$\frac{1}{6}\left\{P_0\left[V_{\mathrm{od}}\left(\mathcal{L}\mathcal{L}(V_{\mathrm{od}})^2 V_{\mathrm{od}} - 2\mathcal{L}\mathcal{L}(V_{\mathrm{od}})V_{\mathrm{od}}\mathcal{L}(V_{\mathrm{od}}) + \mathcal{L}V_{\mathrm{od}}\mathcal{L}(V_{\mathrm{od}})^2\right)\right]P_0\right. \tag{114}$$
$$\left. + P_0\left[-\mathcal{L}\left(\mathcal{L}(V_{\mathrm{od}})^2 V_{\mathrm{od}}^2 + 2\left(\mathcal{L}(V_{\mathrm{od}})V_{\mathrm{od}}\right)^2 - V_{\mathrm{od}}\mathcal{L}(V_{\mathrm{od}})^2 V_{\mathrm{od}}\right)\right]P_0\right\}$$

$$= \left[\sum_{p=\pm}p\frac{J^4}{3}\left(\frac{18}{(U+p\varepsilon_T)^3} + \frac{14}{U^2(U+p\varepsilon_T)} + \frac{14}{U(U+p\varepsilon_T)^2}\right)\right.$$
$$\left. + p\frac{J^2 J_{\mathrm{c}}^2}{6}\left(\frac{2}{(U+p\varepsilon_T)^3} + \frac{14}{U^2(U+p\varepsilon_T)} + \frac{14}{U(U+p\varepsilon_T)^2}\right)\right]S^z\,.$$

Adding the correction terms up to fourth order in the perturbation $\hat{V}$ to the Hamiltonian describing the lead degrees of freedom we arrive at the effective low-energy Hamiltonian $H_{\mathrm{eff}}^{(4)}$ which reads

$$H_{\mathrm{eff}}^{(4)} = h(U,\varepsilon_T)S^z + \tilde{h}(U,\varepsilon_T)S_{\mathrm{res}}^z + J_z(U,\varepsilon_T)S^z S_{\mathrm{res}}^z + J_\perp(U,\varepsilon_T)(S^x S_{\mathrm{res}}^x + S^y S_{\mathrm{res}}^y) \tag{115}$$
$$+ \sum_{k,\sigma}\varepsilon_k c_{k,\sigma}^\dagger c_{k,\sigma} + \theta(-t)\frac{V}{2}\sum_{k,\sigma,\sigma'}c_{k,\sigma}^\dagger \tau_{\sigma\sigma'}^x c_{k,\sigma}\,,$$

where $h(U,\varepsilon_T)$ constitutes an effective magnetic field on the impurity and incorporates all terms coupling to $S^z \otimes \mathbf{1}_r$, $\tilde{h}(U,\varepsilon_T)$ denotes the terms proprotional to $\mathbf{1}_d \otimes S_{\mathrm{res}}^z$, and $J_z(U,\varepsilon_T)$ and $J_\perp(U,\varepsilon_T)$ feature all terms coupling the impurity spin and the lead spins in the z-direction or x-y-direction respectively. This effective model is reminiscent of the anisotropic single-channel Kondo model with anisotropic coupling between lead spins and impurity spin in the z-direction and the x-y-plane as well as a magnetic field $h(\varepsilon_T) \simeq \mathcal{O}(\varepsilon_T)$ on the impurity. In our effective model the spin degrees of freedom do not correspond to physical spins. Instead, we identify pseudo-spins $|\downarrow\rangle \equiv |g\rangle$ and $|\uparrow\rangle \equiv |e\rangle$ on the impurity. For vanishing bias voltage, $V = 0$, we can identify $|\downarrow\rangle$ with the antisymmetric and $|\uparrow\rangle$ with symmetric modes in the leads. The operators creating these modes read

$$c_{\uparrow,k}^\dagger = \frac{1}{\sqrt{2}}\left(c_{\mathrm{L},k}^\dagger + c_{\mathrm{R},k}^\dagger\right)\,, \tag{116}$$
$$c_{\downarrow,k}^\dagger = \frac{1}{\sqrt{2}}\left(c_{\mathrm{L},k}^\dagger - c_{\mathrm{R},k}^\dagger\right)\,.$$

For finite bias voltage, $V \neq 0$, the term

$$\frac{V}{2}\sum_{k,\sigma,\sigma'}c_{k,\sigma}^\dagger \tau_{\sigma,\sigma'}^x c_{k,\sigma'}\,, \tag{117}$$

leads to a hybridization of these two modes, which means they are no longer eigenstates of the lead Hamiltonian. The conserved quantum number becomes the lead index $\alpha = L, R$ instead. The linear dependance between lead index α and pseudo-spin index σ in the leads proves to be responsible for differing properties, e.g. decay rates, of our effective model as compared to the anisotropic Kondo model.

Schrieffer-Wolff transformation of the current operators

To determine how the operator representing the ring current I_{r} couples to to the matrix elements of the reduced impurity density matrix ρ_{ns} we perform a second Schrieffer-Wolff transformation up to leading order in J^2/U. From

this we obtain an effective ring current operator I_{eff} acting in the subspace P_0. The operators measuring the local currents in the ring were previously defined as

$$I_{\text{r}} = I_{\text{u}} - I_{\text{l}},\tag{118}$$

$$I_{\text{u}} = -i\,[n_2, H] = ieJ\left(d_1^\dagger d_2 - d_2^\dagger d_1\right),\tag{119}$$

$$I_{\text{l}} = -i\,[n_3, H] = ieJ\left(d_1^\dagger d_3 - d_3^\dagger d_1\right).\tag{120}$$

The Schrieffer-Wolff of the current operators has been performed in the same fashion as the transformation for the effective Hamiltonian. The resulting effective ring current operator in leading order reads

$$I_{\text{r,eff}} = P_0 \exp(S)\left(I_{\text{u}} - I_{\text{l}}\right)\exp(-S)P_0 \simeq P_0\left(1 + \mathcal{L}(V_{\text{od}})\right)\left(I_{\text{u}} - I_{\text{l}}\right)\left(1 - \mathcal{L}(V_{\text{od}})\right)P_0\tag{121}$$

$$= J^2\left(\frac{2}{U} + \frac{1}{U - \varepsilon_T} + \frac{1}{U + \varepsilon_T}\right)S^y.$$

One consequently finds that $(I_{\text{r,eff}})_{\uparrow,\downarrow} = (I_{\text{eff}})_{\downarrow,\uparrow}^\dagger \propto J^2/U$ and $(I_{\text{r,eff}})_{\downarrow,\downarrow} = (I_{\text{eff}})_{\uparrow,\uparrow} \equiv 0$. The effective current operator couples exclusively to the off-diagonal matrix elements $\rho_{\uparrow,\downarrow}$ and $\rho_{\downarrow,\uparrow}$ of the reduced impurity density matrix ρ_{ns} in the context the effective low-energy decription. The transient decay rate of the ring current is therefore determined by the decay rate of these two particular matrix elements.

In contrast, the current, which is transmitted through the ring, is equivalent to

$$I_{\text{t}} = I_{\text{u}} + I_{\text{l}},\tag{122}$$

as the sum of the two local currents amounts to the total current flowing from one lead through the ring to the second lead. Using the effective operators for the local currents I_{u} and I_{l} after a Schrieffer-Wolff transformation, we find for the transmitted current in leading order the effective operator

$$I_{\text{t,eff}} = J^2\left(\frac{2}{U} - \frac{1}{U - \varepsilon_T} - \frac{1}{U + \varepsilon_T}\right)S^y.\tag{123}$$

It is immediately obvious that the effective operator for the transmitted current $I_{\text{t,eff}} \to 0$ for $U/\varepsilon_T \to \infty$. As a consequence, the coupling of the transmitted current to the off-diagonal elements of the effective reduced density matrix, which are the ones exhibiting the small decay rate, is strongly suppressed for strong interaction. This is consistent with our numerical data from tdDMRG, where we also do not observe a slow decay of the transmitted current, but a decay on the time scale given by the hybridization Γ_0.

Limitations on the viability of the effective low-energy model

As a consistency check of the effective model $H_{\text{eff}}^{(4)}$ up to order U^{-4} we perform a series expansion of the perturbative corrections in U^{-n} around $U/J \to \infty$. The results of this series expansion for the amplitudes of the spin-spin interaction terms read

$$J_z = 2J^2 J_{\text{c}}^2 \sum_{p=\pm} \frac{5}{U^3} + \frac{1}{U^2(U + p\varepsilon_T)} + \frac{2}{U(U + p\varepsilon_T)^2} + \frac{2}{(U + p\varepsilon_T)^3} \simeq \frac{10}{U^3}J^2 J_{\text{c}}^2 + \mathcal{O}\left(U^{-4}\right),\tag{124}$$

$$J_\perp = -2J^2 J_{\text{c}}^2 \sum_{p=\pm} \frac{p}{U^2(U + p\varepsilon_T)} - \frac{p}{U(U + p\varepsilon_T)^2} - \frac{3p}{(U + p\varepsilon_T)^3} \simeq 0 + \mathcal{O}\left(U^{-5}\right).\tag{125}$$

When expanding the expression for $J_\perp$ up to fourth order in the inverse interaction strength U^{-1} we encounter an inconsistoncy of our Schrieffer-Wolff transformation as $J_\perp$ vanishes up to this order. We can therefore not assume with certainty that the spin-spin interaction $J_\perp$ in the effective model is finite.

Perturbation theory for the effective model in the limit $T \to 0$

In our effective model the hybridization between the impurity and the leads satisfies

$$\sqrt{\Gamma_0} \propto \max(J_z, J_\perp) \propto \mathcal{O}(J^2 J_{\text{c}}^2/U^3),\tag{126}$$

which is small in the limit $U \gg \max(J, \varepsilon)$ even in the case of a chosen bare coupling $J_c = \mathcal{O}(J)$. In the limit $U/\varepsilon \gg 1$ we can thus perform a perturbation theory calculation for the effective low-energy model whilst employing the same values for the bare model parameters J, J_c as in our initial DMRG calculations. This way we can compare the results from both methods for the decay rate of the off-diagonal matrix elements $\rho_{\uparrow,\downarrow}$ and $\rho_{\downarrow,\uparrow}$ and thus the decay rate of the transient ring current in the strong interaction limit. In contrast to the earlier perturbation theory calculation, we no longer study charge fluctuations on the impurity but pseudo-spin fluctuations instead. This requires a few modifications to the procedure outlined in the previous section on the perturbation theory. The coupling Liovilliain L_V now features two field superoperators for the leads and the impurity, instead of just one. It reads

$$L_V = G_{12}^{p_1 p_2} : J_1^{p_1} J_2^{p_2} :, \tag{127}$$

where

$$G_{12}^{p_1 p_2} A = \delta_{p_1 p_2} \begin{cases} d_1 d_2 A & p_1 = + \\ -A d_1 d_2 & p_1 = - \end{cases} . \tag{128}$$

The field superoperators for the leads remain unchanged

$$J_1^p A = \begin{cases} c_1 A & p = + \\ A c_1 & p = - \end{cases} . \tag{129}$$

As a consequence, the first order corrections to the Liouvillian now contain two reservoir contractions $\gamma_{11'}^{pp'}$ which in turn requires integration over two reservoir frequencies ω_1 and ω_2. The perturbative correction reads

$$\Sigma^{(1)}(E) = \sum_{p_1 p_2 p_3 p_4} \sum_{1234} G_{12}^{p_1 p_2} \frac{1}{E_{12} + \bar{\omega}_{12} - L_{\mathrm{ns}}} G_{34}^{p_3 p_4} \gamma_{14}^{p_1 p_4} \gamma_{23}^{p_2 p_3} . \tag{130}$$

It is again possible to separate the corrections into a symmetric and an antisymmetric part. In the zero temperature limit the two contributions read

$$\Sigma_s(E) = \frac{1}{4} \sum_{\nu_1, \eta_1} \sum_{\nu_2, \eta_2} \bar{G}_{12} \int_{-\infty}^{\infty} d\omega_1 d\omega_2 \, \rho(\omega_1)\rho(\omega_2) \frac{1 + \mathrm{sign}(\omega_1)\, \mathrm{sign}(\omega_2)}{E + \omega_1 + \omega_2 + \eta_1 \mu_1 + \eta_2 \mu_2 - L_{\mathrm{ns}}} \bar{G}_{\bar{2}\bar{1}} , \tag{131}$$

$$\Sigma_a(E) = -\frac{1}{2} \sum_{\nu_1, \eta_1} \sum_{\nu_2, \eta_2} \bar{G}_{12} \int_{-\infty}^{\infty} d\omega_1 d\omega_2 \, \rho(\omega_1)\rho(\omega_2) \frac{\mathrm{sign}(\omega_2)}{E + \omega_1 + \omega_2 + \eta_1 \mu_1 + \eta_2 \mu_2 - L_{\mathrm{ns}}} \tilde{G}_{\bar{2}\bar{1}} . \tag{132}$$

First we discuss the integrals over the reservoir frequencies ω_1 and ω_2. For this we introduce the density of states

$$\rho(\omega) = 2\rho_0 \theta(\omega - |D|) . \tag{133}$$

The integral in the symmetric part of the self-energy correction evaluates to

$$
\begin{aligned}
\int_{-\infty}^{\infty}\int_{-\infty}^{\infty} d\omega_1 d\omega_2 \, \frac{\rho(\omega_1)\rho(\omega_2)}{4} \frac{1 + \mathrm{sign}(\omega_1)\mathrm{sign}(\omega_2)}{z + \omega_1 + \omega_2} &= \rho_0^2 \left(\int_{-D}^{0}\int_{-D}^{0} d\omega_1 d\omega_2 \frac{1}{z + \omega_1 + \omega_2} \right. \\
&\quad \left. + \int_{0}^{D}\int_{0}^{D} d\omega_1 d\omega_2 \frac{1}{z + \omega_1 + \omega_2} \right) \\
&= \rho_0^2 \left[2z \log z + (z - 2D) \log(z - 2D) \right. \\
&\quad + 2(z - D)\log(z - D) - 2(z + D)\log(z + D) \\
&\quad \left. + (z + 2D)\log(z + 2D) \right] \\
&\simeq \rho_0^2 \left[2z \log z + (z - 2D)\left(i\pi + \log D + \log 2 - \frac{z}{2D} \right) \right. \\
&\quad + (z + 2D)\left(\log D + \log 2 + \frac{z}{2D} \right) \\
&\quad - 2(z + D)\left(\log D + \frac{z}{D} \right) \\
&\quad \left. + 2(-z + D)\left(i\pi + \log D - \frac{z}{D} \right) \right] \\
&\simeq \rho_0^2 \left[2z \log\left(\frac{2z}{D} \right) - 2z - i\pi z \right] \\
&= \rho_0^2 \left[2z \log\left(\left| \frac{2z}{D} \right| - 1 \right) - i\pi |z| \right] .
\end{aligned}
\tag{134}
$$

Similarly, the integral in the antisymmetric self-energy correction gives

$$-\int_{-\infty}^{\infty}\int_{-\infty}^{\infty}d\omega_1 d\omega_2 \frac{\rho(\omega_1)\rho(\omega_2)}{2}\frac{\text{sign}(\omega_2)}{z+\omega_1+\omega_2} = -\int_{-D}^{D}2d\omega_1\left(\int_{0}^{D}\frac{\rho_0^2 d\omega_2}{z+\omega_1+\omega_2} - \int_{-D}^{0}\frac{\rho_0^2 d\omega_2}{z+\omega_1+\omega_2}\right) \tag{135}$$

$$= -2\rho_0^2\left\{\int_{-D}^{D}d\omega_1\left[-\log(\omega_1+z)+\log(\omega_1+z-D)\right]\right.$$

$$\left. +\int_{-D}^{D}d\omega_1\left[-\log(\omega_1+z)+\log(\omega_1+z+D)\right]\right\}$$

$$= -2\rho_0^2\left[2(z-D)\log(z-D)-2(z+D)\log(z+D)\right.$$

$$\left. -(z-2D)\log(z-2D)+(z+2D)\log(z+2D)\right]$$

$$\simeq -2\rho_0^2\left[2(z-D)\left(i\pi+\log D-\frac{z}{D}\right)\right.$$

$$-2(z+D)\left(\log D+\frac{z}{D}\right)$$

$$+(z+2D)\left(i\pi+\log D+\log 2-\frac{z}{2D}\right)$$

$$\left. -(z-2D)\left(i\pi+\log D+\log 2-\frac{z}{2D}\right)\right]$$

$$\simeq -2\rho_0^2\left(i\pi z+4D\log 2\right).$$

Next, we discuss the superoperators acting in the Liouville space of the impurity. We follow the notation introduced in Schoeller and Reininghaus [Phys. Rev. B **80**, 045117 (2009)]. First we define the Liouville superoperators that act as the spin operators $\underline{S}=(S^x,S^y,S^z)$ on the impurity. These Liouville superoperators are

$$\underline{L}^{\pm}=(L^{\pm x},L^{\pm y},L^{\pm z}), \tag{136}$$

where the sign $p=\pm$ indicates the order of the operators as

$$\underline{L}^+ A=\underline{S}A \quad , \quad \underline{L}^- A=-A\underline{S}. \tag{137}$$

A matrix representation of these superoperators in the basis $|\uparrow\uparrow\rangle, |\downarrow\downarrow\rangle, |\uparrow\downarrow\rangle, |\downarrow\uparrow\rangle$ reads

$$L^{+x}=\begin{pmatrix}0&0&0&\frac{1}{2}\\0&0&\frac{1}{2}&0\\0&\frac{1}{2}&0&0\\\frac{1}{2}&0&0&0\end{pmatrix}, \quad L^{+y}=\begin{pmatrix}0&0&0&-\frac{i}{2}\\0&0&\frac{i}{2}&0\\0&-\frac{i}{2}&0&0\\\frac{i}{2}&0&0&0\end{pmatrix}, \quad L^{+z}=\begin{pmatrix}\frac{1}{2}&0&0&0\\0&-\frac{1}{2}&0&0\\0&0&\frac{1}{2}&0\\0&0&0&-\frac{1}{2}\end{pmatrix}, \tag{138}$$

$$L^{-x}=-\begin{pmatrix}0&0&\frac{1}{2}&0\\0&0&0&\frac{1}{2}\\\frac{1}{2}&0&0&0\\0&\frac{1}{2}&0&0\end{pmatrix}, \quad L^{-y}=\begin{pmatrix}0&0&0&-\frac{i}{2}\\0&0&\frac{i}{2}&0\\0&-\frac{i}{2}&0&0\\\frac{i}{2}&0&0&0\end{pmatrix}, \quad L^{-z}=\begin{pmatrix}\frac{1}{2}&0&0&0\\0&-\frac{1}{2}&0&0\\0&0&\frac{1}{2}&0\\0&0&0&-\frac{1}{2}\end{pmatrix}. \tag{139}$$

From these superoperators we can construct a basis of superoperators sufficient to describe the spin-spin interaction processes between impurity and lead pseudo-spins. We further introduce the 'scalar' superoperators

$$L^a=\frac{3}{4}\mathbf{1}+\underline{L}^+\cdot\underline{L}^-, \tag{140}$$

$$L^c=\frac{1}{2}\mathbf{1}+2L^{+z}L^{-z},$$

$$L^h=L^{+z}+L^{-z},$$

as well as the vector superoperators

$$\underline{L}^1=\frac{1}{2}\left(\underline{L}^+-\underline{L}^--2i\underline{L}^+\times\underline{L}^-\right), \tag{141}$$

$$\underline{L}^2=-\frac{1}{2}\left(\underline{L}^++\underline{L}^-\right),$$

$$\underline{L}^3=\frac{1}{2}\left(\underline{L}^+-\underline{L}^-+2i\underline{L}^+\times\underline{L}^-\right).$$

Due to the anisotropy of the interactions we need to introduce a third set of superoperators, which reads

$$
\begin{aligned}
L_\pm^4 &= L^{2x} \pm iL^{2y} \pm \left[\left(L^{+x} \pm iL^{+y} \right) L^{-z} + L^{+z} \left(L^{-x} \pm iL^{-y} \right) \right] , \\
L_\pm^5 &= L^{2x} \pm iL^{2y} \mp \left[\left(L^{+x} \pm iL^{+y} \right) L^{-z} + L^{+z} \left(L^{-x} \pm iL^{-y} \right) \right] , \\
L_\pm^6 &= L^c \pm \frac{1}{2} \left[\left(L^{3x} + iL^{3y} \right) \left(L^{1x} + iL^{1y} \right) + \left(L^{3x} - iL^{3y} \right) \left(L^{1x} - iL^{1y} \right) \right] .
\end{aligned}
\tag{142}
$$

In terms of these basis superoperators the bare Liouvillian is given as

$$
L_{\mathrm{ns}} = h(U, \varepsilon_T) L^h ,
\tag{143}
$$

where $h(U, \varepsilon_T)$ is the effective magnetic field on the impurity and L^h represents the action of $[S^z, \bullet]$ on the impurity. The effective Liouvillian for the impurity in first order perturbation theory reads

$$
L_{\mathrm{eff}}(E) = L_{\mathrm{ns}} + \Sigma^{(1)}(E) .
\tag{144}
$$

The first order, energy-dependent self-energy corrections are

$$
\begin{aligned}
\Sigma^{(1)}(E) =& \rho_0^2 \sum_{\substack{\nu_1,\eta_1 \\ \nu_2,\eta_2}} \bar{G}_{12} \left[2(E + \mu_{12} - L_{\mathrm{ns}}) \left(\log \left| \frac{2(E + \mu_{12} - L_{\mathrm{ns}})}{D} \right| - 1 \right) \right] \bar{G}_{\bar{2}\bar{1}} \\
&+ \rho_0^2 \sum_{\substack{\nu_1.\eta_1 \\ \nu_2,\eta_2}} \bar{G}_{12} \left[-i\pi \left| E + \mu_{12} - L_{\mathrm{ns}} \right| \right] \bar{G}_{\bar{2}\bar{1}} \\
&+ \rho_0^2 \sum_{\substack{\nu_1,\eta_1 \\ \nu_2,\eta_2}} \bar{G}_{12} \left[-8D \log 2 - 2\pi i (E + \mu_{12} - L_{\mathrm{ns}}) \right] \tilde{G}_{\bar{2}\bar{1}} ,
\end{aligned}
\tag{145}
$$

where $\mu_{12} = \eta_1 \mu_1 + \eta_2 \mu_2$ and

$$
\bar{G}_{12} = \begin{cases} +J_\perp \left(\tau_{\sigma_1 \sigma_2}^x L^{2x} + \tau_{\sigma_1 \sigma_2}^y L^{2y} \right) + J_z \tau_{\sigma_1 \sigma_2} L^{2z} & \eta_1 = -\eta_2 = + \\ -J_\perp \left(\tau_{\sigma_2 \sigma_1}^x L^{2x} + \tau_{\sigma_2 \sigma_1}^y L^{2y} \right) - J_z \tau_{\sigma_2 \sigma_1} L^{2z} & \eta_1 = -\eta_2 = - \end{cases} ,
\tag{146}
$$

as well as

$$
\tilde{G}_{12} = \begin{cases} +J_\perp \left[\tau_{\sigma_1 \sigma_2}^x \left(L^{1x} + L^{3x} \right) + \tau_{\sigma_1 \sigma_2}^y \left(L^{1y} + L^{3y} \right) \right] + J_z \tau_{\sigma_1 \sigma_2} \left(L^{1z} + L^{3z} \right) & \eta_1 = -\eta_2 = + \\ -J_\perp \left[\tau_{\sigma_2 \sigma_1}^x \left(L^{1x} + L^{3x} \right) + \tau_{\sigma_2 \sigma_1}^y \left(L^{1y} + L^{3y} \right) \right] - J_z \tau_{\sigma_2 \sigma_1} \left(L^{1z} + L^{3z} \right) & \eta_1 = -\eta_2 = - \end{cases} .
\tag{147}
$$

It is then straightforward to calculate the self energy corrections that are proportional to simple products $\bar{G}_{12} \bar{G}_{\bar{2}\bar{1}}$ and $\bar{G}_{12} \tilde{G}_{\bar{2}\bar{1}}$. The two different products of superoperators evaluate to

$$
\begin{aligned}
\bar{G}_{12} \bar{G}_{\bar{2}\bar{1}} =& \sum_j \bar{G}_{12} |v_j)(v_j| \bar{G}_{\bar{2}\bar{1}} \\
=& \frac{J_\perp^2}{2} L^c + \frac{J_\perp^2}{2} L^c + J_\perp^2 (L^a - L^c) + \frac{J_z^2}{2} (L^c + L^h) + J_\perp^2 (L^a - L^c) + \frac{J_z^2}{2} (L^c - L^h) ,
\end{aligned}
\tag{148}
$$

and

$$
\bar{G}_{12} \tilde{G}_{\bar{2}\bar{1}} = \sum_j \bar{G}_{12} |v_j)(v_j| \tilde{G}_{\bar{2}\bar{1}} = \frac{J_\perp^2}{2} L^h - \frac{J_\perp^2}{2} L^h + J_\perp^2 L^{3z} - J_\perp^2 L^{3z} .
\tag{149}
$$

To calculate terms involving $\bar{G} f(\mu_{12}) \bar{G}$ and $\bar{G} f(\mu_{12}) \tilde{G}$ a rotation to a different basis is necessary.

Modifications to the perturbation theory for spin fluctuations due to the linear dependence between pseudo-spin and lead index

From eq. (113) we see that the magnetic field $\tilde{h}(U, \varepsilon_T)$, experienced by the pseudo-spins on the lead sites closest to the impurity, is small up to order $\mathcal{O}(U^{-4})$, ie $h^* \ll h, V$ and we can thus neglect it. It is then more useful to express the Hamiltonian in the basis of the lead index $\alpha \in \{L, R\}$ eigenstates, which corresponds to a rotation $\tau_{\sigma_1 \sigma_2}^x \to \tau_{\alpha_1 \alpha_2}^z$,

$\tau^y_{\sigma_1\sigma_2} \to -\tau^y_{\alpha_1\alpha_2}$, $\tau^z_{\sigma_1\sigma_2} \to \tau^x_{\alpha_1\alpha_2}$ in the leads. In terms of the rotated operators, $c_{\alpha,k} = 1/\sqrt{2}(c_{\downarrow,k} \pm c_{\uparrow,k})$, the effective Hamiltonian reads

$$H^{(4)}_{\text{eff}} = hS^z + \sum_{k,\alpha} \varepsilon_k c^\dagger_{k,\alpha} c_{k,\alpha} + \frac{V}{2} \sum_{k,\alpha,\alpha'} c^\dagger_{k,\alpha} \tau^z_{\alpha\alpha'} c_{k,\alpha'} \tag{150}$$
$$+ \frac{J_z}{2} \sum_{\substack{k,k' \\ \alpha,\alpha'}} S^z c^\dagger_{k,\alpha} \tau^x_{\alpha\alpha'} c_{k',\alpha'} + \frac{J_\perp}{2} \sum_{\substack{k,k' \\ \alpha,\alpha'}} c^\dagger_{k,\alpha} c_{k',\alpha'} (S^x \tau^z_{\alpha\alpha'} + S^y(-\tau^y_{\alpha\alpha'}))\,.$$

In this rotated basis the part of the Hamiltonian acting exclusively on the leads is diagonal so the reservoir contractions reduce to simple fermionic distribution functions. After rotation the vertex superoperators read

$$\bar{G}_{12} = \begin{cases} + \left[J_\perp L^{2x} \tau^z_{\alpha_1\alpha_2} + J_\perp L^{2y}(-\tau^y_{\alpha_1\alpha_2}) + J_z L^{2z} \tau^x_{\alpha_1\alpha_2}\right] & \eta_1 = -\eta_2 = + \\ - \left[J_\perp L^{2x} \tau^z_{\alpha_2\alpha_1} + J_\perp L^{2y}(-\tau^y_{\alpha_2\alpha_1}) + J_z L^{2z} \tau^x_{\alpha_2\alpha_1}\right] & \eta_1 = -\eta_2 = - \end{cases}\,, \tag{151}$$

and

$$\tilde{G}_{12} = \begin{cases} + \left[J_\perp (L^{1x} + L^{3x}) \tau^z_{\alpha_1\alpha_2} + J_\perp (L^{1y} + L^{3y})(-\tau^y_{\alpha_1\alpha_2}) + J_z (L^{1z} + L^{3z}) \tau^x_{\alpha_1\alpha_2}\right] & \eta_1 = -\eta_2 = + \\ - \left[J_\perp (L^{1x} + L^{3x}) \tau^z_{\alpha_2\alpha_1} + J_\perp (L^{1y} + L^{3y})(-\tau^y_{\alpha_2\alpha_1}) + J_z (L^{1z} + L^{3z}) \tau^x_{\alpha_2\alpha_1}\right] & \eta_1 = -\eta_2 = - \end{cases}\,, \tag{152}$$

where we have dropped the factor $1/2$ resulting from the substitution $S_{\sigma_1\sigma_2} \to \tau_{\alpha_1\alpha_2}$ for convenience. We reintroduce the factor in the final result. The first set of self-energy corrections that are affected by the linear dependance between pseudo-spin index and lead index involve terms proportional to $\bar{G}_{12}\mu_{12}\bar{G}_{\bar{2}\bar{1}}$ and $\bar{G}_{12}\mu_{12}\tilde{G}_{\bar{2}\bar{1}}$. The first term reads

$$\bar{G}_{12}\mu_{12}\bar{G}_{\bar{2}\bar{1}} = \sum_{\alpha_1,\alpha_2} \sum_{\eta_1=-\eta_2} \sum_{l,k=x,y,z} \tau^l_{\alpha_1\alpha_2} \tau^k_{\alpha_2\alpha_1} L^{2l} \left(\eta_1 V_{\alpha_1} + \eta_2 V_{\alpha_2}\right) L^{2k}\,. \tag{153}$$

In the following we evaluate the cases $l = k$ and $l \neq k$ separately. For each example calculation we set $\eta_1 = -\eta_2 = +$ without loss of generality. For $l = k$ we find

$$\bar{G}_{12}\mu_{12}\bar{G}_{\bar{2}\bar{1}} = J^2_l \sum_{\substack{\alpha_1,\alpha_2=1,2 \\ l=x,y,z}} \tau^l_{\alpha_1\alpha_2} \tau^l_{\alpha_2\alpha_1} \left(V_{\alpha_1} - V_{\alpha_2}\right) L^{2l} L^{2l} \tag{154}$$
$$= J^2_l \sum_{\substack{\alpha_1,\alpha_2=1,2 \\ l=x,y,z}} \tau^l_{\alpha_1\alpha_2} \tau^l_{\alpha_2\alpha_1} \left[\text{sign}(V_{\alpha_1})(1 - \delta_{\alpha_1\alpha_2})\right] L^{2l} L^{2l}$$
$$= J^2_l V \sum_{l=x,y,z} \left[\text{sign}(V_2)\tau^l_{21}\tau^l_{12} + \text{sign}(V_1)\tau^l_{12}\tau^l_{21}\right] L^{2l} L^{2l} = 0\,,$$

and for $l \neq k$ we obtain

$$\bar{G}_{12}\mu_{12}\bar{G}_{\bar{2}\bar{1}} = J_l J_k \sum_{\substack{l \neq k \\ l,k=x,y,z}} \sum_{\alpha_1,\alpha_2=1,2} \tau^l_{\alpha_1\alpha_2} \tau^k_{\alpha_2\alpha_1} \left[\text{sign}(V_{\alpha_1})(1 - \delta_{\alpha_1\alpha_2})\right] L^{2l} L^{2k} \tag{155}$$
$$= J_l J_k V \sum_{\substack{l \neq k \\ l,k=x,y,z}} \left[\text{sign}(V_2)\tau^l_{21}\tau^k_{12} + \text{sign}(V_1)\tau^l_{12}\tau^k_{21}\right] L^{2l} L^{2k}$$
$$= (J_z J_\perp) V L^{2x}\,.$$

This term, proportional to the bias voltage V, does not appear in the perturbation theory of the regular anisotropic Kondo model. The correction term still satisfies $\text{Tr}_S(L^{2x}) = 0$ such that $\text{Tr}_S(L_{\text{eff}}) = 0$, a necessary requirement for the validity of the perturbation theory. Similarly for $\bar{G}_{12}\mu_{12}\tilde{G}_{\bar{2}\bar{1}}$ we find

$$\bar{G}_{12}\mu_{12}\tilde{G}_{\bar{2}\bar{1}} = J_l J_k \sum_{\substack{l \neq k \\ l,k=x,y,z}} \sum_{\alpha_1,\alpha_2=1,2} \tau^l_{\alpha_1\alpha_2} \tau^k_{\alpha_2\alpha_1} \left[\text{sign}(V_{\alpha_1})(1 - \delta_{\alpha_1\alpha_2})\right] L^{2l} \left(L^{1k} + L^{3k}\right) \tag{156}$$
$$= J_l J_k V \sum_{\substack{l \neq k \\ l,k=x,y,z}} \left[\text{sign}(V_2)\tau^l_{21}\tau^k_{12} + \text{sign}(V_1)\tau^l_{12}\tau^k_{21}\right] L^{2l} \left(L^{1k} + L^{3k}\right)$$
$$= (J_z J_\perp) V L^{3x}\,,$$

which satisfies $\text{Tr}_S(L^{3x}) = 0$ as well. Next we discuss the correction terms proportional to $\bar{G}_{12}|E + \mu_{12} - L_{\text{ns}}|\bar{G}_{\bar{2}\bar{1}}$. We know that $\Gamma_0 \ll h$ which means that the perturbative corrections to the roots of the unperturbed Liovillian L_{ns} are small. We can thus safely assume $\lambda_{\pm}^* = L_{\text{eff}}(\lambda_{\pm}^*) \simeq \pm h$. As such we evaluate the correction terms proportional to $\bar{G}_{12}|E + \mu_{12} - L_{\text{ns}}|\bar{G}_{\bar{2}\bar{1}}$ for $E \simeq \pm h$ and obtain

$$
\begin{aligned}
\bar{G}_{12}|h + \mu_{12} - L_{\text{ns}}|\bar{G}_{\bar{2}\bar{1}} =& J_l J_k \sum_{\substack{\alpha_1,\alpha_2=1,2 \\ l,k=x,y,z}} \tau_{\alpha_1\alpha_2}^l \tau_{\alpha_2\alpha_1}^k L^{2l} |h - L_{\text{ns}} + \eta_1 V_{\alpha_1} + \eta_2 V_{\alpha_2}| L^{2k} \\
=& \frac{J_\perp^2}{4}\left(|h+V| + |h-V|\right) L_+^6 + \frac{J_\perp^2}{2}|h|L_-^6 \\
&+ \frac{J_\perp^2}{4}\left(2|\delta h| + |\delta h + V| + |\delta h - V|\right)(L^a - L^c) \\
&+ \frac{J_\perp^2}{4}\left(2|2h| + |2h + V| + |2h - V|\right)(L^a - L^c) \\
&+ \frac{J_\perp J_z}{4}\left(|\delta h + V| - |\delta h - V|\right)\left(L_-^4 + L_+^5\right) \\
&+ \frac{J_\perp J_z}{4}\left(|2h + V| - |2h - V|\right)\left(L_+^4 + L_-^5\right) \\
&+ \frac{J_z^2}{4}\left(|\delta h + V| + |\delta h - V|\right)\left(L^c + L^h\right) \\
&+ \frac{J_z^2}{4}\left(|2h + V| + |2h - V|\right)\left(L^c - L^h\right),
\end{aligned}
\tag{157}
$$

where $\delta h = h - h_0$ and we verify that $\text{Tr}_S(L_{\pm}^4) = \text{Tr}_S(L_{\pm}^5) = \text{Tr}_S(L_{\pm}^6) = 0$. Lastly we discuss the correction term that involves the logarithm of the Liouvillian L_{ns}. We abbreviate $z = E + \mu_{12} - L_{\text{ns}}$ and approximate $E = \pm h$. The correction term then evaluates to

$$
\begin{aligned}
\bar{G}_{12} z \log\left|\frac{2z}{D}\right| \bar{G}_{\bar{2}\bar{1}} =& \frac{J_\perp^2}{4} h \log\left|\frac{2h}{D}\right| L_-^6 \\
&+ \frac{J_\perp^2}{4}\left((h+V)\log\left|\frac{2(h+V)}{D}\right| + (h-V)\log\left|\frac{2(h-V)}{D}\right|\right) L_+^6 \\
&+ \frac{J_\perp^2}{4}\left(\delta h \log\left|\frac{2\delta h}{D}\right| + (2h)\log\left|\frac{4h}{D}\right|\right)(L^a - L^c) \\
&+ \frac{J_z^2}{4}\left((\delta h+V)\log\left|\frac{2(\delta h + V)}{D}\right| + (\delta h-V)\log\left|\frac{2(\delta h - V)}{D}\right|\right)\left(L^c + L^h\right) \\
&+ \frac{J_z^2}{4}\left((2h+V)\log\left|\frac{2(2h + V)}{D}\right| + (2h-V)\log\left|\frac{2(2h - V)}{D}\right|\right)\left(L^c - L^h\right) \\
&+ \frac{J_z J_\perp}{4}\left((\delta h+V)\log\left|\frac{2(\delta h + V)}{D}\right| - (\delta h-V)\log\left|\frac{2(\delta h - V)}{D}\right|\right)\left(L_-^4 + L_+^5\right) \\
&+ \frac{J_z J_\perp}{4}\left((2h+V)\log\left|\frac{2(2h + V)}{D}\right| - (2h-V)\log\left|\frac{2(2h - V)}{D}\right|\right)\left(L_+^4 + L_-^5\right) \\
&+ \frac{J_\perp^2}{4}\left((\delta h+V)\log\left|\frac{2(\delta h + V)}{D}\right| + (\delta h-V)\log\left|\frac{2(\delta h - V)}{D}\right|\right)(L^a - L^c) \\
&+ \frac{J_\perp^2}{4}\left((2h+V)\log\left|\frac{2(2h + V)}{D}\right| + (2h-V)\log\left|\frac{2(2h - V)}{D}\right|\right)(L^a - L^c).
\end{aligned}
\tag{158}
$$

With all the self-energy terms evaluated we can determine the eigenvalues of the effective Liouvillian $L_{\text{eff}}(E)$. To obtain an analytical result for the roots $\pm h$ we perform the diagonalization of L_{eff} perturbatively as well. In first order

$$
h^{(1)} = (\uparrow\downarrow |L_{\text{eff}}(h)| \uparrow\downarrow) = -(\downarrow\uparrow |L_{\text{eff}}(-h)| \downarrow\uparrow),
\tag{159}
$$

we find

$$h = h_0 + \frac{\rho_0^2}{4} \left[-2 \left(J_\perp^2 h + J_z^2 \delta h \right) + \frac{J_\perp^2}{2} h \log \left| \frac{2h}{D} \right| \right. \tag{160}$$

$$+ \frac{J_\perp^2}{2} \left((h+V) \log \left| \frac{2(h+V)}{D} \right| + (h-V) \log \left| \frac{2(h-V)}{D} \right| \right)$$

$$+ J_z^2 \left((\delta h + V) \log \left| \frac{2(\delta h + V)}{D} \right| + (\delta h - V) \log \left| \frac{2(\delta h - V)}{D} \right| \right)$$

$$\left. - i \frac{\pi}{4} J_\perp^2 \left(|h+V| + |h-V| + 2|h| \right) - i \frac{\pi}{2} J_z^2 \left(|\delta h + V| + |\delta h - V| \right) \right] ,$$

where $\delta h = h - h_0 \simeq 0$ and h_0 denotes the root of the bare Liouvillian L_{ns}. The imaginary part of the root h, which corresponds to its transient decay rate, reads

$$\mathrm{Im}(h) \simeq -i\rho_0^2 \frac{\pi}{16} J_\perp^2 \left(|h+V| + |h-V| + 2|h| \right) - i\rho_0^2 \frac{\pi}{8} J_z^2 \left(|\delta h + V| + |\delta h - V| \right) . \tag{161}$$

We see that for $V \to 0$ the imaginary part of h is essentially given by the terms proportional to $J_\perp^2$. For $V = 0$ we thus find a power law decrease of the decay rate with $U^{-\alpha}$ and $\alpha \geq 8$. For finite bias voltage and $U \to \infty$ the terms proportional to J_z^2 become dominant and we observe a power law decrease of the decay rate with $U^{-\beta}$ and $\beta = 6$. In figure 14 we plot our numerical results for the decay rates $\mathrm{Im}(\lambda_\pm^*)$ with $\lambda_\pm^* = \pm h$. We find that for $V = 0$ the decay rates obey a power law, $\mathrm{Im}(\lambda_\pm^*)(U) \propto U^{-8}$, the same as the spin-flip interaction $J_\perp^2(U)$. For finite bias voltage we observe a different power law, $\mathrm{Im}(\lambda_\pm^*)(U) \propto U^{-6}$, a behavior shared by $J_z^2(U)$. Our numerical findings support our perturbative result for the decay rates (161). The perturbation theory for the effective model finds that $\Gamma \to 0$ for $U \to \infty$ and supports our findings from DMRG calculations and perturbation theory in the limit of small coupling which see very long life times $\tau \gg \Gamma_0^{-1}$ of the ring current oscillations.
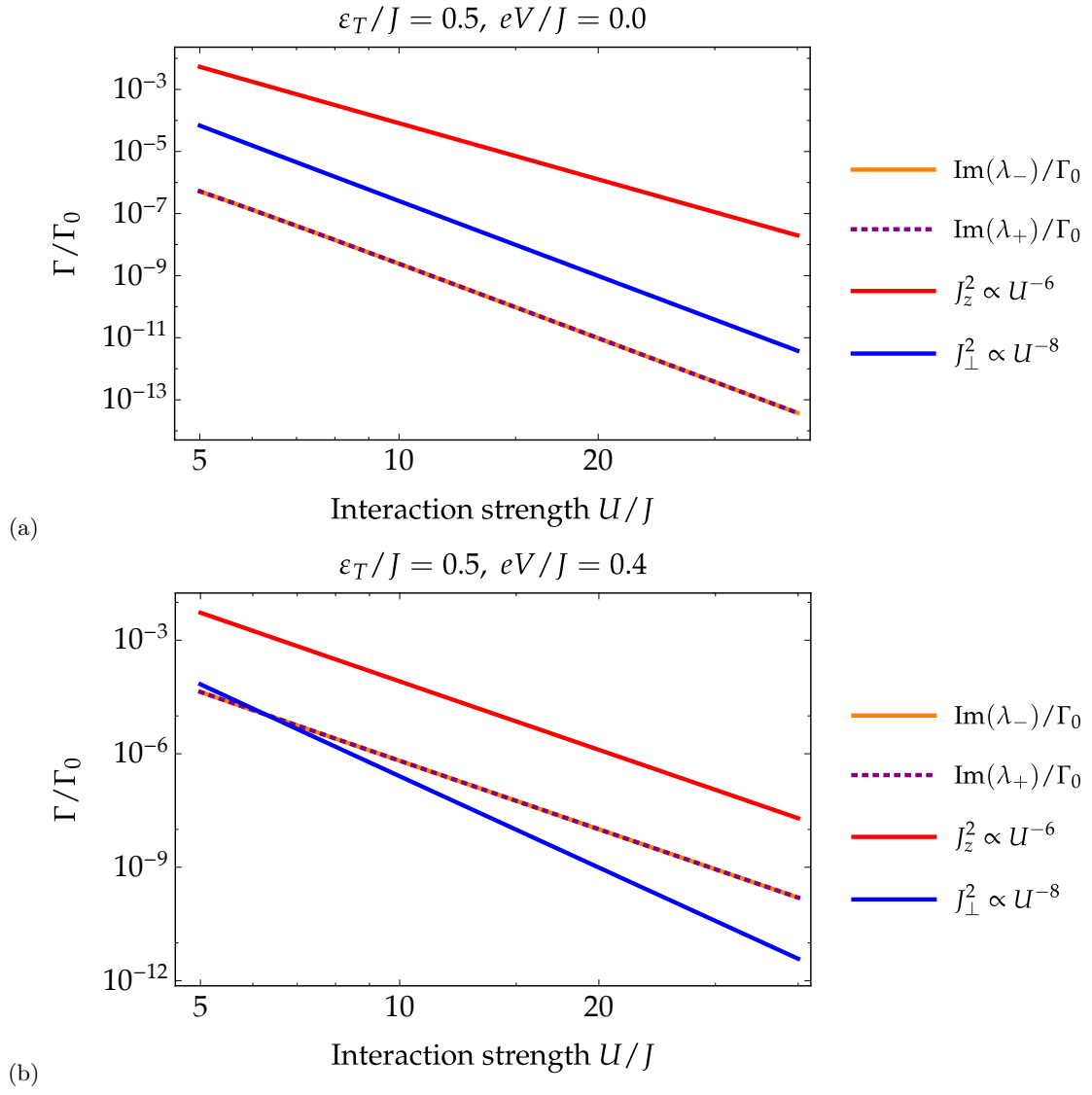
FIG. 14. Decay rate Γ/Γ_0 of the roots λ_+ and λ_- for (a): $\varepsilon_T/J = 0.5$, $J_c/J = 0.5$, $eV/J = 0$ and (b): $\varepsilon_T/J = 0.5$, $J_c/J = 0.5$, $eV/J = 0.4$.